



UNIVERSITY
OF TRENTO

Master's degree in Mechatronics Engineering a.y. 2023/2024

Mechanical design for mechatronics

CLEANING AND HAIL PROTECTION SYSTEM FOR SOLAR PANELS

Prof. Emiliano Rustighi

Group 17: Filippo Avi, Alberto Giora, Matteo Manzini, Edoardo Murgia, Andrea Silvan

INDEX

1. **Introduction:** Panels damage due to hail
2. **Product design specification:**
 - 2.1 Recognize the needs
 - 2.2 Problem statement
 - 2.3 Concept generation from specifications
 - 2.4 Concept selection
3. **Design Process**
4. **Final design Proposal**
 - 4.1 Subunit01: Panel protection
 - 4.2 Subunit02: Panel cleaning
 - 4.3 Subunit03: Motor generation and transmission
 - 4.4 Subunit04: Detection and sensing
 - 4.5 Subunit05: Support and anchoring
5. **Device Analysis and verification**
 - 5.1 Motor generation and transmission
 - 5.2 Design and verification of the user shaft
 - 5.3 Couplings design
 - 5.4 Rod rope support
 - 5.5 The cleaning system
6. **Project review**
7. **Conclusion and annexes**
8. **Reference and appendices**

1 INTRODUCTION: PANELS DAMAGE DUE TO HAIL

Due to climate change the importance of solar panels as a sustainable energy source has grown. Consequently, protecting panels from hail and cleaning them has become a challenge.

The importance of panel protection has increased due to the growing frequency in extreme weather phenomena, while panel cleaning is essential for performance that is often compromised by accumulations of sand and dust.

To solve the problem of panels breakage due to hail, the following method are used:

- Financial coverage, so that they are replaced in case of breakage
- Transparent anti-hail nets to minimize the impact on efficiency. Bear in mind that special supports must also be allocated for the resistance of the networks
- High inclination of the panels.

To develop a cost reasoning, the following should be taken into account:

- Average life time of a solar panel
- Probability of breakage by location area (estimates for the calculation of insurance policies)
- Lack of efficiency due to the application of tempered glass. Nowadays photovoltaic panels are designed to withstand adverse weather conditions by covering the photovoltaic cells with a glass panel. This leads to a loss of efficiency due to reflective phenomena. It would be interesting to develop a more efficient and fragile solar panel for a later roller shutter application.
- Recovery of efficiency due to frequent cleaning of the panel. It is usually carried out once a year, especially in marine areas, near trees or close to industrial areas. The daily energy loss over a year caused by dust deposited on the surface could be from 4.4% to 20% when there are long periods without rain.[1]

2 PRODUCT DESIGN SPECIFICATION

2.1 Recognize the needs

The focus of our project is to protect solar panels from damages due to hailstorms.

In addition the system has to be able to autonomously clean the panels, to keep their efficiency as high as possible, without requiring frequent manual maintenance.

Therefore, the idea is to design a roller shutter that can automatically close to shield the panels whenever a hailstorm is detected in the area.

The cleaning mechanism should work even independently with respect to the hail protection, so it could be activated manually in case the panels need to be cleaned.

2.2 Problem statement

The focus of this chapter is the design process. We are evaluating all the design considerations, under the form of requirements and specifications, in order to come up with a few different concepts to compare.

To do this we filled up *Table01* with all the requirements, the specifications they're related to and their numerical values (in case they're explicable).

Table01: design specifications

REQUIREMENTS	SPECIFICATIONS	VALUE
Safety & Regulations(in accordance with the most stringent regional regulations)	<ul style="list-style-type: none">The weight of the shutter <u>must be supported</u> by the roof;according to regional laws, the weight of the structure <u>must not exceed</u> the 10% of the weight of the roof;	<ul style="list-style-type: none">Solar panel weight ~ $15,8 \frac{kg}{m^2}$Weight of a cement roof ~ $440 \frac{kg}{m^2}$Max weight of the structure ~ $(440)0,1 - 15,8 = 28,2 \frac{kg}{m^2}$
The dimensions of the shutter should accommodate all the standard measures of solar panels arrays	<ul style="list-style-type: none">Tailored structure to accommodate all the standard panel sizes organized in two modules;	<ul style="list-style-type: none">1st module <u>width</u> range: $0,80 \div 1,10 [m]$;1st module <u>length</u> range: $1,55 \div 3,30 [m]$;2nd module <u>width</u> range: $1,60 \div 2,30 [m]$;2nd module <u>length</u> range: $1,55 \div 3,33 [m]$;
High efficiency in protecting the solar panels against hailstorms	<ul style="list-style-type: none">High resistance of shutter material;Quick reaction time in order to close the shutter before the hailstorm reaches the panels;	<ul style="list-style-type: none"><u>Resistance</u> of panel cover class 4;The shutter <u>must close</u> completely in a maximum of 60 seconds;
The shutter mechanism must protect the panels only when it is strictly necessary	<ul style="list-style-type: none">Effective hail detection algorithm;The sensors must be able to distinguish between rain and hail;Manual control for opening and closing available;	

The shutter mechanism must be able to clean the panels effectively	<ul style="list-style-type: none"> Low efficiency lost due to dirt after cleaning compared to new panel under controlled illumination; Rotary brushes; 	<ul style="list-style-type: none"> <u>Efficiency lost</u> due to dirt 30% in worst condition; Rotary brushes <u>tangential speed</u> is twice as much the linear one;
The shutter mechanism requires little to no maintenance	<ul style="list-style-type: none"> Guaranteed time before maintenance; Cleaning water source (house pipeline, optional); 	<ul style="list-style-type: none"> <u>10 years</u> before maintenance for the structure; <u>5 years</u> before maintenance for the eventual net;
Required energy supply and Data connection	<ul style="list-style-type: none"> Powered by Standard household energy supply; Controlled via Wi-Fi connection; 	<ul style="list-style-type: none"> 220V 50Hz;
The shutter mechanism can be seamlessly mounted in array configuration	<ul style="list-style-type: none"> Can be mounted on panels close to each other; The structure must minimize the shadow projected onto the panels below; 	<ul style="list-style-type: none"> Panel separation < 5cm; < 2% <u>shadow</u> on panel surface;
The structure can withstand various weather conditions for many years	<ul style="list-style-type: none"> Water resistant; Sun damage resistant; 	<ul style="list-style-type: none"> IP67;

2.3 Concept generation by specification

Starting from the specifications established in the previous table, we came up with a total of three different design concepts. All three satisfy the project boundaries, but in different ways.

CONCEPT 01: Roller shutter with rigid slats

The sketch of concept 01 is represented in *Figure01* where the major components are shown. The *Table02* summarizes all the main technical features of the design.

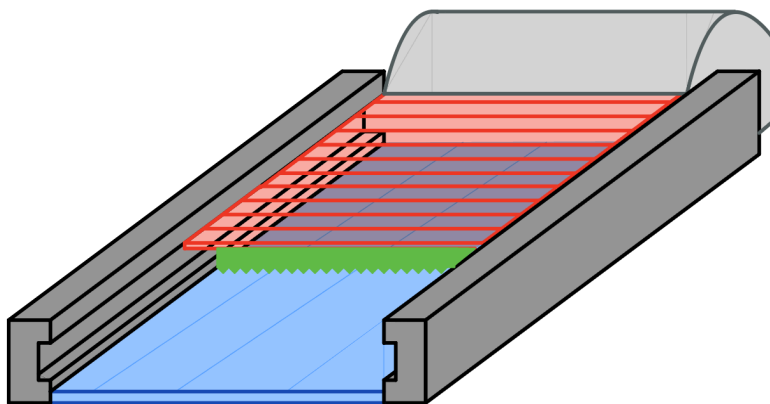


Figure01: Sketch of concept01

Table02: design concept01 description

PART	FUNCTION	REALIZATION
PROTECTION	Panel protection	<ul style="list-style-type: none"> • Rolling shutter
CLEANING	Panel cleaning	<ul style="list-style-type: none"> • Fixed brush
MOTION	Motion generation	<ul style="list-style-type: none"> • 220V 50Hz electric motor
	Motion transmission	<ul style="list-style-type: none"> • Epicyclic gearing
	Panel protection system motion constraining	<ul style="list-style-type: none"> • Shutter rails
WATER	Water supply	<ul style="list-style-type: none"> • House pipeline (optional)
	Water dispensing	<ul style="list-style-type: none"> • Directly on cleaning mechanism (optional)

ACTIVATION	Detection and sensing	<ul style="list-style-type: none"> • Manual actuation: <ul style="list-style-type: none"> ◦ Bluetooth ◦ WiFi • Internal sensors (optical laser precipitation sensor)
FIXING	Support and anchoring	<ul style="list-style-type: none"> • Anchoring to preexisting panel supports • Anchoring to newly installed supports

CONCEPT 02: Folding shutter with rigid slats

The sketch of concept 2 is represented in *Figure02* where the major components are shown. The *Table04* summarizes all the main technical features of the design.

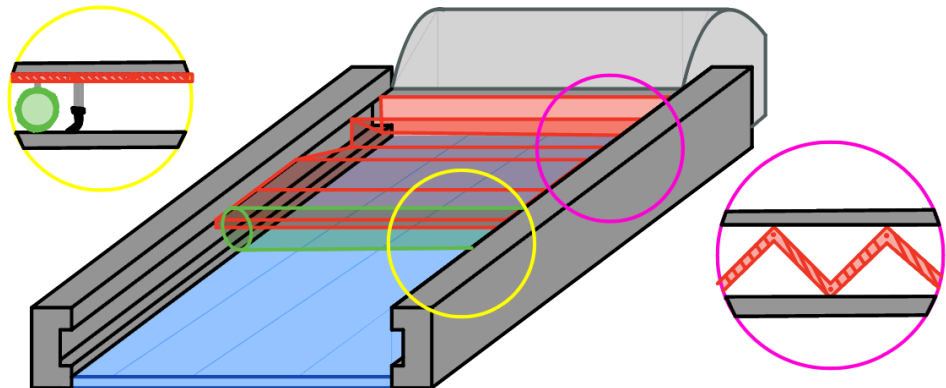


Figure02:Sketch of concept02

Table03: design concept02 description

PART	FUNCTION	REALIZATION
PROTECTION	Panel protection	<ul style="list-style-type: none"> • Folding shutter
CLEANING	Panel cleaning	<ul style="list-style-type: none"> • Rolling brush • Rubber wiper
MOTION	Motion generation	<ul style="list-style-type: none"> • 220V 50Hz electric motor
	Motion transmission	<ul style="list-style-type: none"> • Belt transmission (actuator on listing arm)
	Panel protection system motion constraining	<ul style="list-style-type: none"> • Shutter rails

WATER	Water supply	<ul style="list-style-type: none"> • House pipeline (optional)
	Water dispensing	<ul style="list-style-type: none"> • Water spray nozzles (optional)
ACTIVATION	Detection and sensing	<ul style="list-style-type: none"> • Manual actuation: <ul style="list-style-type: none"> ◦ Bluetooth ◦ WiFi • Internal sensors (optical laser precipitation sensor)
FIXING	Support and anchoring	<ul style="list-style-type: none"> • Anchoring to preexisting panel supports • Anchoring to newly installed supports

CONCEPT 03: Roller shutter with anti-hail net

The sketch of concept03 is represented in *Figure03* illustrating its major components. The *Table04* summarizes all the main technical features of the design.

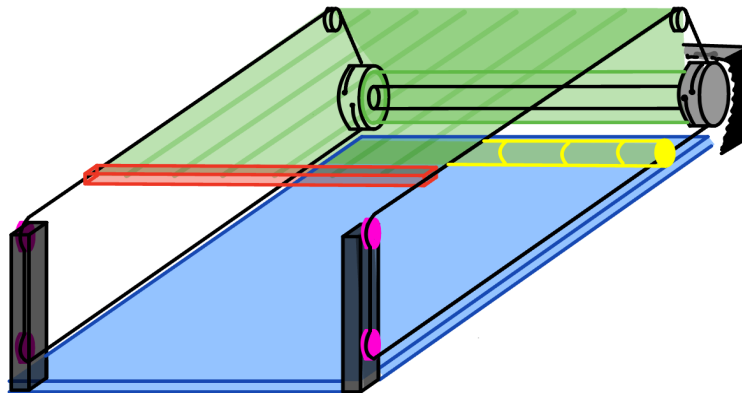


Figure 03: Sketch of concept03

Table04: design concept03 description

PART	FUNCTION	REALIZATION
PROTECTION	Panel protection	<ul style="list-style-type: none"> • Anti-hail net
CLEANING	Panel cleaning	<ul style="list-style-type: none"> • Rolling brush
MOTION	Motion generation	<ul style="list-style-type: none"> • 220V 50Hz electric motor
	Motion transmission	<ul style="list-style-type: none"> • Stainless cables transmission
	Panel protection system motion	<ul style="list-style-type: none"> • Cables pulleys

	constraining	
WATER	Water supply	<ul style="list-style-type: none"> • House pipeline (optional)
	Water dispensing	<ul style="list-style-type: none"> • Directly on cleaning mechanism (optional)
ACTIVATION	Detection and sensing	<ul style="list-style-type: none"> • Manual actuation: <ul style="list-style-type: none"> ◦ Bluetooth ◦ WiFi • Internal sensors (optical laser precipitation sensor)
FIXING	Support and anchoring	<ul style="list-style-type: none"> • Anchoring to preexisting panel supports • Anchoring to newly installed supports

2.4 Concept selection

In *Table05* is illustrated the decision matrix of the tree concepts. Among the three proposals, the Roller shutter with anti-hail net project proved to be the most effective in respecting the project specifications.

Table05:decision matrix

REQUIREMENTS LIST	IMPORTANCE	CONCEPT		
		Concept 01	Concept 02	Concept 03
Safety & Regulations	4	9	8	10
Can fit the standard measures of solar panels	7	7	5	10
Effective at protecting against hailstorms	10	10	10	8
The shutter mechanisms protects the panel only when strictly necessary	7	3	3	10
Is able to clean the panels effectively	9	4	10	10
Requires little to no maintenance	6	10	7	4
Energy supply and Data connection	5	10	10	10
Can be mounted in an array configuration without problems	8	10	3	7
The structure can withstand the weather for many years	8	10	10	6
		512	474	528

3.DESIGN PROCESS

The design process of the system components is described in detail in the analysis and verification section. Here we provide a brief overview of the sequences that led us to design the two main mechanisms.

3.1 Net mechanism

Main steps are listed:

1. We started deciding the unrolling speed of the net needed to cover the solar panels as fast as possible. After that, we calculated the necessary preload of the net to withstand the hail.
2. The required power of the motor to be applied to the shaft was estimated from the speed of the mechanism and the preload tension; even the work of the weight force due to the cleaning system was taken into account.
3. Then was made the engine selection and transmission design.
4. After this choice, we determined the values of the diameter of the net roller cylinder and of the rope drums; those are fundamental for the study of the forces that are needed to reach the preload, acting on the shaft.
5. Subsequently, the shaft force analysis was carried out for the first time and the minimum diameter has been determined. For brevity this first iteration will not be exposed in the report.
6. Once the ideal diameter was chosen, bearings and parallel keys were sized, and shoulders were selected.
7. Following that, the force study was conducted for the second time, considering the motor torque as an unknown.
8. Once the force data of the spur gears were found, the force analysis was performed again, for the third time, with the aim of finding the critical points on the shaft.
9. In the end, the minimum diameter of the shaft was checked (taking into account the notching effects) and the stiffness was verified with FEM analysis.

3.2 Cleaning system

Main steps are listed:

1. At the first step, similar commercial applications and documents that study solar panel cleaning were analyzed.
2. Based on the initial analysis, the primary parameters of the cleaning system and the brush to be used were selected.
3. Starting with the necessary characteristics for effectively cleaning the solar panel and the chosen brush, we then selected the electric motor, its coupling, and the bearings for the rotating brush.
4. Next, the mechanism to move the system along the solar panel was defined, and the general shape of the carrier system was designed.
5. A decision was made to use the steel cable already present along the solar panel (needed for the protection system) to transmit the motion of the cart to reduce the complexity and the amount of parts needed. For this purpose the impact of the cleaning subunit on the rest of the system was then studied, the force needed to drag the cart along the panel and the power consumed were fixed.
6. Based on the selected carrier system and on the movement and speed it should have, the constraining system was selected. A series of wheels that directly ride along the panel and some rollers that prevent the system from derailing will be installed on the cart for this purpose.
7. A system to keep the brush pressed against the panel to increase the cleaning effectiveness was implemented through the use of a helicoidal spring, and the geometry of the cleaning subunit was finalized.
8. Lastly we added a cover to protect the most vulnerable parts from atmospheric conditions.

4 FINAL DESIGN PROPOSAL

To best describe how the design works, the individual subunits mentioned in the project specifications will be described in the next chapters

4.1 Panel protection

One of the two main purposes of the system is to protect solar panels from damage due to hail or other hydrometeors, so the design of a reliable and effective protection subunit is of primarily importance. The technology selected through the decision matrix to perform this task is a hail net, since it is a readily available product, already used worldwide to protect plantations and known for its reliability. Moreover, it is very light and has the added benefit of not completely blocking the sunlight from hitting the surface of the protected panel; in fact, even when it is fully extended over it, the net only blocks between 5-13% of the sunlight, depending on the net type and color.

The downsides of this solution, that should be borne in mind when designing the system, are due to the fact that the net is flexible:

- An extension/retraction and rolling/unrolling system, used to deploy it from the closed position and back, is necessary.
- The net will bend under the weight of the hail and will consequently need a correctly designed support and tensioning system.

Another factor to bear in mind, is the maintenance of a hail net: a standard agrarian implementation can resist more than 5 years, but since in this specific application the net is stored away from atmospheric conditions for the majority of the time the maintenance should be minimal, mainly depending on the amount of hail it has to block.

Hail nets have already been used to protect solar panels, but a system to only keep it over the panels when necessary in order to gain efficiency has never been adopted.

Hail net selection

A standard hail net is made of threaded HDPE that has relatively good mechanical properties (analyzed in depth later).

From the paragraph studying the deformation and preload of the net is visible that a standard HDPE hail net is perfectly suitable to this application, so the following product shown in *Figure04* was selected

Product Specification

Catalogue No:		Product Description:		
31010141101		Cristal net 5040 leno		
CHARACTER	UNIT	SPECIFICATION REQUIREMENT	STANDARD	REMARKS
MATERIAL		HDPE		
COLOUR	--	clear		
SHADE FACTOR	%	8.5 - 13	ASTM D 1746	
AVERAGE WEIGHT	g/Sq.M	55 - 60	ASTM D 3776	
BREAKING STRENGTH Warp	Kg/5cm	47+	ASTM D 5034	
BREAKING STRENGTH Weft	Kg/5cm	34+	ASTM D 5034	
HOLE SIZE	mm.	2.26 x 3.55		CALCULATED VALUE
YARN DIAMETER	mm.	0.27-0.28		
YARN DENSITY - WARP	cm	2.6 X 2		
YARN DENSITY - WEFT	cm	3.9 - 4.1	Visual Inspection	
YARN DENSITY - WARP X WEFT	INCH	13.3 X 10.2		
UV STABILITY	Kly	700	ASTM G 154	

Figure04: Net product specifications

The relevant properties of this net are the clear color, to block less sunlight, the average weight of 55-60 g/m² and a breaking strength of 67 N/cm under traction.

4.2 Panel cleaning

The second purpose of the system is to keep the solar panel clean in order to increase its overall efficiency.

Through a study performed on similar commercial applications and their effectiveness, a rolling nylon brush was selected, as it is the most commonly used brush and one of the most effective for cleaning solar panels. This brush needs to be rotated at a certain speed to effectively clean the surface of the panel. However, this type of brush is most effective at cleaning the panel in presence of water so the mechanism should be actuated when there is rainwater present on the panel to increase the efficiency gained through cleaning. The brush will also need to be lightly pressed against the solar panel to effectively clean it.



Figure 05: examples of solar panel cleaning systems

A study of the literature on rotating brushes [6][7] revealed the difficulty of analytically modelling the characteristics of the brush, which are impossible to exactly model without proper lab testing of the selected brush to obtain the drag coefficient, bristle number and distribution etc.

Similar commercial applications (see examples in *Figure 05*) and papers that discuss solar panel cleaning [8][9] were then studied to obtain some approximatives values for our application of the rotation speed needed to clean the panel and of the power absorbed by the brush while dragging along the surface of the panel and by the system that carries the brush along the panel:

- The brush should rotate at around $200 \frac{\text{rev}}{\text{min}}$ with a minimum of $60 \frac{\text{rev}}{\text{min}}$ while under load.
- A system for rotating the brush with the dimensions needed for this application needs 3 [Nm] to effectively rotate the cleaning brush.

The general structure of the mechanism was then defined: one subunit should be responsible for rotating the brush at the correct speed to clean the panel, while another subunit should carry the rotating brush along the panel to clean all the exposed area.

Carrier mechanism definition

It was decided to directly couple the actuation of the cart carrying the brush to the actuation of the net extending mechanism to reduce the number of parts, the overall complexity of the system and the number of electric motors needed by connecting it to the steel cable responsible for extending and tensioning the net.

This has some noteworthy consequences:

- When the net is extended/retracted the cleaning system cart is also dragged along the surface of the solar panel and the brush is rotated through the use of its separate electric motor to perform a cleaning cycle of the panel.
- When the net is retracted the cart with the cleaning system is parked at the opposite end of the solar panel, so a system for protecting the brush from the weather is needed.

The cart is going to be constrained to the solar panel through some wheels that sit directly over and under the frame of the panel and some rollers to keep the cart centered along the actuation axis, leaving some space between them and the panel to not overconstrain the mechanism.

Rotation mechanism definition

For the rotation of the brush it was decided to use a separate electric motor instead of coupling it to the actuation of the carrier in order to simplify the mechanical aspects of the structure, to decouple the cleaning of the panel from the deployment of the net and to be able to tweak the rotation of the brush without modifying other parts of the mechanism.

This creates the need to transmit power to the motor present on the carrier, and in order to do that a cable drag energy chain has been chosen to prevent any possible entanglements.

The brush will be rotated in the upward direction of the solar panel to help sustain the weight of the whole system against gravity so the force generated by its friction against the panel will help the actuation of the carrier instead of acting against it.

It is noted that a nylon brush wears and gets consumed during the period of its usage, so its diameter will slightly reduce, so a mechanism to compensate for this diameter reduction will need to be employed.

The cleaning mechanism and its components will be discussed in detail and dimensioned step by step in its dedicated section in the Design Process section of this document.

4.3 Motor generation and transmission

The motion transmission must be simple and resistant, given that the field of application requires both outdoor exposure and absence of maintenance.

The mesh covering system adds a complication compared to transmission using rigid slats. In fact, for similar applications, usually only the rotation of the rolling shutter shaft is used, thus unrolling the rods along a straight guide. This operation would be ineffective with the net, since with the rotation of the shaft alone, the net cannot follow the rectilinear guide, as it is not made up of rigid elements.

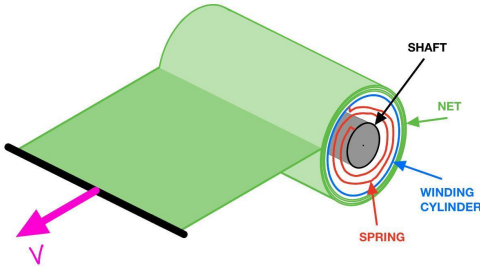


Figure06: Unrolling sketch

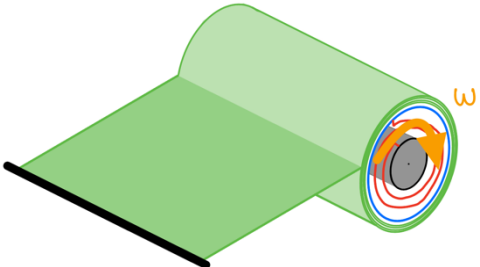


Figure07: Rolling sketch

To overcome the problem, the motion transmission system was completely redesigned. The relaxation of the net will be achieved by a traction force: a rigid rod connected to the final edge of the net will be pulled by a system of ropes, equipped with a return drum. So the aim will therefore be to activate the mechanism by imposing a linear speed v chosen from specifications as shown in *Figure06*. The winding will instead be carried out by the rotation of the shaft, which will recall the net to the spool, in this case the speed set will be that of rotation ω of the shaft as shown in the *Figure07*.

The system described requires careful synchronization between the rolling and unrolling motions, as there could be a risk of jamming the net, or, on the contrary, excessively stretching it. In the design process chapter, an analysis will be conducted on the ideal diameter of the drum and the winding of the net, at most torsional springs will be used in order to always have a minimum tension of the net, and therefore avoid jamming of the same.

4.4 Detection and sensing

Digitron ZDM-100 disdrometer was chosen for the application in question. It's about an optical measurement system using modern laser technology and it detects essential information to identify precipitation hydrometeors, including speed, size and quality of individual particles.

The working principle of ZDM is a laser sensor that can emit a horizontal beam and its components are: laser generator or emitted, laser beam, laser receiver and rainfall particles (*Figure08*).

It is possible to map the speed and size of hydrometeors allowing 32 types of precipitation to be classified.

Data acquisition and encapsulation is enabled by a digital signal processor.

Installation

The installation position is important to ensure maximum measurement precision and quality. The choice of the best location depends on two factors: vibrations and hemisphere. When it must be installed in the North Hemisphere, the receiving end is preferable in the south, otherwise the emitting end is installed in the north. In the case of the southern, the position will be the opposite.

This choice is made because the interface from sunlight can cause interference problems with the receiving laser. If the influence of all these factors is not completely excluded, false rain and/or fog particles may be detected.

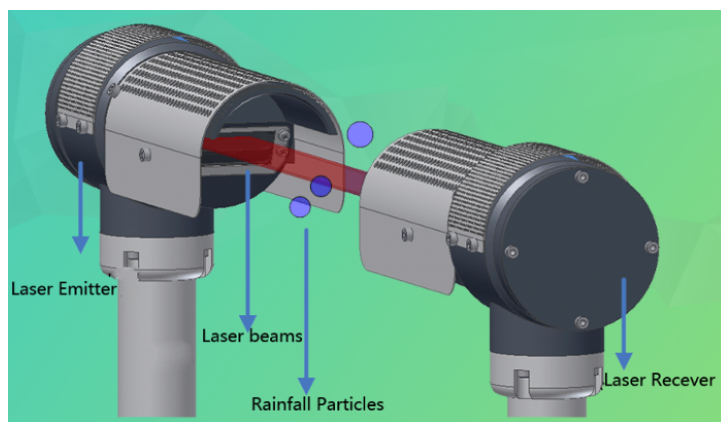


*Figure08:*Digitron ZDM-100 disdrometer

Meteor classification

The analysis of the parameters to classify the hydrometeors is managed by the variation in the output voltage and allows it to be related on the type of precipitation.

When no particles passes through the laser, the output voltage of receiver remains at maximum (around 13 V).

As the precipitation passes through the laser beam, the voltage decreases so that the diameter of the hydrometeor can be determinated.

The falling speed of the single particle is calculated according to the time of voltage drop. Based on the diameter and speed of fall it is possible to determinate and distinguish hail from other precipitations.

The device also contains a temperature sensor which is placed on the head of the device. To prevent it from freezing or fogging up, the disdrometer has an internal heating mechanism if the recorded temperature is less than 12 °C.

Dati in output

When the disdrometer has been installed with an earthed socket, it must be connected to a calculator using the Recommended Standard 485 communication cable.

The latter is chosen as it is shielded and carries the signal on the wires (twisted pair): the first transmits the original signal while the second its inverse copy to reduce interference.

It is ideal for long distance use and electrically noisy environments.

The client will open the software from the calculator and through this it will be possible to open the connection with the disdrometer (server) via the ports.

The port number is on which the hosting server is listening.

There is also an interference adapter that allows automatic protocol conversion between ZDM and client. You can connect the interference adapter with ZDM and connect the former to the PC.

Start the monitoring software and configure the sensor, also choosing the monitoring time interval.

Item	Value
Date	
Weather	
Intensity (mm/h)	
M_precipitation (mm)	
M_precipitation (mm)	
Avg diameter (mm)	
Particle (num)	
Avg velocity (m/s)	
Radar ref (dBz)	
M_visibility (m)	
T_visibility (m)	
T_precipitation (mm)	
Device voltage (V)	
Device state	
Detector voltage (V)	
Detector state	
Emitter voltage (V)	
Emitter state	
Heating (A)	
Device Temp (°C)	
Ambient Temp (°C)	
Laser voltage (mV)	
Windows state	
Station	
P_distribution	

Figure09: Data detected by sensor

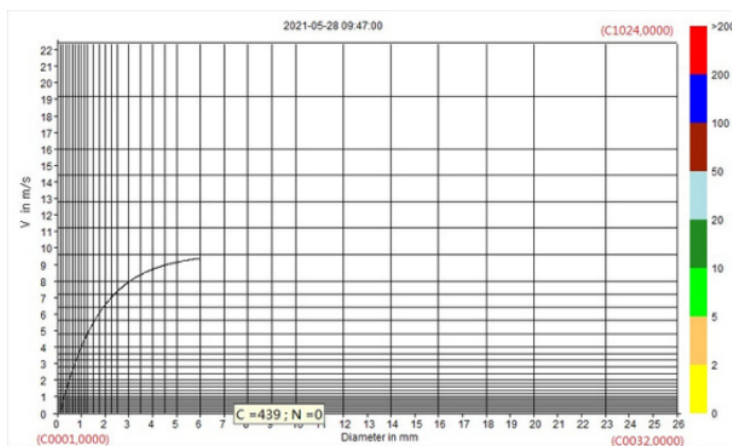


Figure10: Relationship between diameter and falling speed

Figure09 describes all the data that can be detected by the sensors, while the graph (Figure10) represents the relationship between diameter (abscissa) and falling speed (ordinate).

Assuming you have meteors with a diameter greater than 26 [mm], the sensor will assign the maximum size present in the electronic library and send the hydrometeor of maximum size. In our case, the data values for detecting hail are identified by the code 4680 and 4677. WMO Meteorological codes is a table that classified and identified precipitation hydrometeors. The indices that identify the desired precipitation are from 87 to 96.

4.5 Support and anchoring

Each protection module is composed of the drum assembly, where the net is wrapped, the main shaft and the related drives. This block, in length, can be of 2 sizes, for single or double panels, and must be anchored to one of the ends of the column of panels that you want to protect. In addition to this structure, which is the main one, the supports for the return of the steel cable must be fixed, these will be located at the final point of unwinding of the net and this parameter will also depend on which combination of panels you have and on the dimensions of the protective nets that they will choose. The cable will then be mounted once the fixing of these two structures together with the brush assembly has been completed. A summary sketch is shown in the *Figure 11*

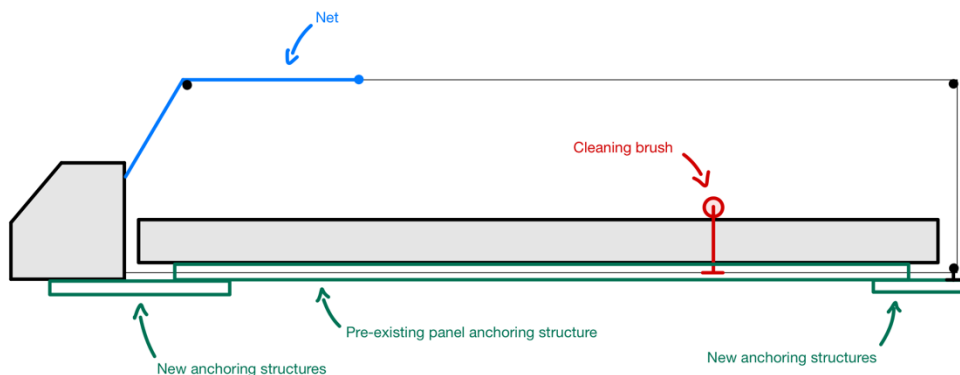


Figure 11: Sketch of support and anchoring system

For the anchoring of these structures it is not possible to identify a single solution, since there are different methods of assembling the panels also depending on the roof/soil on which they are installed. Therefore the preferable solution is to use specific brackets, which are attached to the pre-existing load-bearing structure on which the panels are fixed. In fact, the latter are often made up of standard aluminum guide profiles, on which it is easy and quick to fix and adjust the position of the anchoring points. In this way, installation is also possible on parks of panels installed on the ground. However, it should be noted that this system does not offer high wind resistance, nor a risk of retention of water and snow, therefore its anchoring must be adequate to support only its mass and must not be excessively oversized. This therefore avoids having to have a system structurally designed specifically for this use.

Choice of preloading

Using the following formulas it is possible to calculate the bending deflection f of a cable stretched between two points located at a distance l , represented in *Figure 12*.

- $S = q \cdot l \cdot \frac{1+8n^2}{8n} n = \frac{f}{l}$

To use this formula we approximated the network as a cable, and we calculated the distributed weight force starting from the mass per unit surface area and then calculating the overall weight force.

- $q \cdot l = Q = A \cdot d = 1,1 \text{ [m]} \cdot 3,1 \text{ [m}^2\text{]} \cdot 0,06 \text{ [kg/m}^2\text{]} = 0,20 \text{ [kg]} = 1,96 \text{ [N]}$

Assumed: $s = 200 \text{ [N]}$, the result is $f = 4 \text{ [mm]}$.

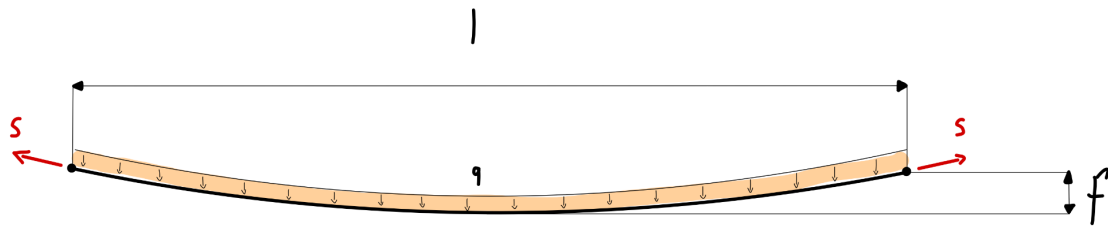


Figure 12: Net deflection scheme

The net does not have a declared stretchability, in fact the material can have high elasticity coefficients but its precise value is difficult to determine. In fact, this is due to countless variables, even those that are not constant over time, such as the decrease in elasticity due to aging from UV rays. For this reason it was necessary to take this aspect into consideration when choosing the type of operation and the related parameters. In addition to this, the variation in size of the net, modifying its weight, is also a variable and therefore the bending caused by its weight force is not always constant. To take all these parameters into consideration, we initially chose to consider the operation of the system without stretching the net, sizing the torsional spring in the drum so that when the net is completely unrolled its weight causes a deflection of only 4 [mm]. A force possibly applied on the net initially causes the spring to completely twist until it mechanically blocks, and subsequently only the elastic coefficient of the net remains with clearance.

The entire system has been sized so as not to have any load applied to the shaft when the net is completely wrapped on the drum and when it is carried out the tension is as low as possible, but which at the same time causes a reduced flexion of the same. The difference in tension between the beginning and the end of unwinding was obtained by using a diameter of the drums on which the cable is wound slightly larger than that on which the net is wound, in this way the linear speed of the free end of the net is slightly greater than the speed unwinding tangential on the drum. By evaluating the breaking load of the net and the maximum torque applicable from the spring, a combination of parameters was found which with a reasonable safety coefficient is effective in all conditions.

Rope study

The cable used to transmit motion and tension the network does not require any particular properties, other than having to resist corrosion, given its exposure to atmospheric agents and the impossibility of

protecting it externally. An optimal choice is to use a 7x(6+1) stranded AISI 316 stainless steel cable with 49 wires, diameter 1.5 [mm]. Its breaking load is 1.27 [kN], more than sufficient for our purpose, as is its elongation, which is negligible for our purposes.

This cable will be wound from both ends in opposite directions on the drum placed on the shaft and integral with it, the dimensions of the slots and the angle of the winding helix have been calculated following the indications of the document [4] approved by Rina.

Drum and spring design

The drum on which the net is wound was chosen with a diameter equal to 80 [mm], this is because with this measurement the difference in diameter during the winding and unwinding of the net can be neglected, due to its thickness, but it allows at the same time to build a fairly compact and not too bulky system.

The torsional spring is a wire spring with a maximum torsional deformation of 360° and a maximum torque of 5.3 [Nm] developed at maximum deformation. Ideally, when the net is unwound, the spring loads through approximately 270°, developing a torque of 4 [Nm].

The spring is attached to the shaft at one end and to the drum on which the net is wound at the other. Once the elongation is complete, the net is tensioned with a force of 200 [N] in total, and the spring has undergone a torsional deformation of precisely 270°, equal to the angular rotation of the drum. If the net is further tensioned, the drum is free to rotate for another approximately 70°, until the imposed limit deformation of the wheel of approximately 340° is reached. At this point the mechanical block intervenes which limits the rotation of the drum and the excessive deformation of the spring which could cause it to break.

5 DEVICE ANALYSIS AND VERIFICATION

This chapter will analyze:

1. The choice of the motor and the coupling to the user shaft: a single motor will activate both the unrolling of the net and the cleaning system. By iteration the most suitable motor will be found, with the aim of not oversizing it to invalidate the efficiency recovered by cleaning.
2. Design and verification of the user shaft, there will be many components and notches such as parallel keys and shoulders.
3. Coupling design
4. Rod rope support. It must be as thin as possible to minimize shadows on the panels.
5. The cleaning system. It must be effective and resistant to satisfy the requirement of no maintenance.

In *Figure 03* the project scheme is reported in order to remind the arrangement of the components.

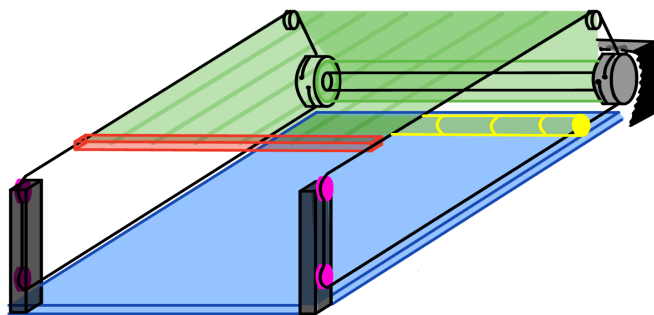


Figure 03: Sketch of concept 03

5.1 Motor generation and transmission

Coupling between the electric motor and the user shaft will be done through spur gears. The nomenclature of diameters and speeds can be clarified from the *Figure13*

By specification, the linear velocity of the net is $v_{net} = 0,15 \frac{m}{s}$ thus the user shaft must have angular velocity $\omega_2 = \frac{v_{net}}{r_{drum}} = \frac{0,15}{0,045} = 3,33 \frac{rad}{s}$.

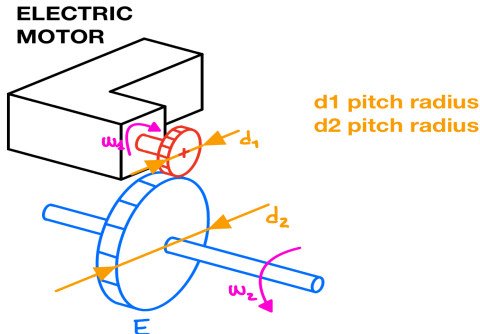


Figure13: Sketch of spur gear transmission

Characteristics of two choice of gearmotors are summarized in the below *Table07*.

Table07: Motor datasheet

Motor datasheet	Power	rpm	η_s	η_d	Torque	k_v	Output shaft diameter
	[W]	$[\frac{rev}{min}]$	[.]	[.]	[Nm]	[.]	[mm]
ECM' 070/030 12E/24E	100	38	0,23	0,57	15	0,8	14
ECM 070/030 12E/24E	100	50	0,31	0,65	12	1,2	14

First of all it's consider the first choice of motor ECM' 070/030 12E/24E. The pinion gear ratio (*on Shaft01*) and the gear (*on Shaft02*) is $\tau' = \frac{\omega_2}{\omega_1} = 0,84$ assumed $\omega'_1 = \frac{2\pi \cdot 38}{60} = 3,98 \frac{rad}{s}$.

Calculate the minimum diameter d_{min} of the pinion, considering hardened and tempered C40 steel, $\tau_s = 220 \text{ [MPa]}$ and safety factor $\Phi = 2$:

- I estimate the minimum diameter $d_{min} = \sqrt[3]{\frac{16T\Phi}{\pi\tau_s}} = 8,86 \text{ [mm]}$.
- Minimum number of teeth $z_{min} = \frac{2\tau k_s}{-1 + \sqrt{1 + \tau(2 + \tau)\sin^2(\alpha)}} = 12,82$, thus $z_{min} = 13$.
- Minimum module value is $m_{min} = \frac{d_{min}}{z_{min}} = 0,53$

The distance between the two shafts must be greater than the drum shaft mounted on the driven shaft and the overall dimensions of the engine, of which the technical drawing is shown in the *Figure 14*.

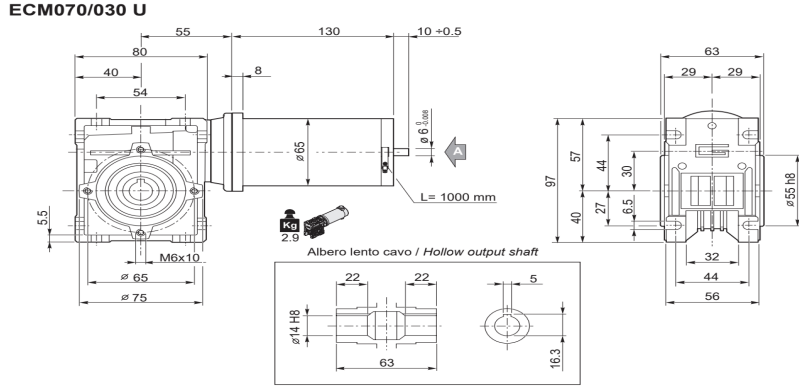


Figure 14: Technical motor draw

We therefore have the condition $R_1 + R_2 = i \leq oo' = r_{drum} + \frac{80}{2} = 85 \text{ [mm]}$

If the value $d_1 = 76 \text{ [mm]}$ is imposed and module $m = 2$ selected, the computations lead to

- $z'_1 = \frac{d_1}{m} = \frac{74}{2} = 37$, thus $z'_2 = \frac{z'_1}{\tau} = \frac{37}{2} = 44,05 \approx 44$
- $d_2 = mz_2 = 88 \text{ [mm]}$, $d_1 = 74 \text{ [mm]}$; $i = \frac{d_1+d_2}{2} = 81 \text{ [mm]}$
-

Overall dimensions not respected, I choose a motor with faster revs, in order to have a smaller pinion and a larger driven wheel. So it's selected ECM 070/030 12E/24E with $n = 50 \text{ [rev/min]}$. The calculations will be reported quickly, without the interactions that have been made.

- Motor velocity now is $\omega_1 = \frac{2\pi 50}{60} = 5,24 \text{ [rad/s]}$, thus $\tau = \frac{\omega_2}{\omega_1} = 0,64$
- It's chosen $d_1 = 72 \text{ [mm]}$, thus $z'_1 = \frac{d_1}{m} = \frac{72}{2} = 36$
- $z'_2 = \frac{z'_1}{\tau} = \frac{36}{0,64} = 56,25 \approx 56$
- Thus the dimensions are $d_2 = mz_2 = 112 \text{ [mm]}$, $d_1 = 72 \text{ [mm]}$
- It's verified $R_1 + R_2 = i = 92 \leq oo' = r_{drum} + \frac{80}{2} = 85 \text{ [mm]}$

Recommended values are $9 \leq \lambda \leq 14$ for the band width, was chosen $w = m\lambda = 20 \text{ [mm]}$.

- $a = m = 2 \text{ [mm]}$ Addendum
- $b = 1,25 m = 2,5 \text{ [mm]}$ Dedendum
- $r_p = \frac{m}{3} = 0,67 \text{ [mm]}$ Fillet radius

Data in the *Table08* are summarized, a UNI 6587 type tooth is considered.

Table08: Pinion and gear dimension

	Module	Pitch diameter	n°teeth	band width	Addendum	Dedendum	Fillet radius
	$m[mm]$	$d[mm]$	z	$w[mm]$	$a[mm]$	$b[mm]$	r_p
Pignon d_1	2	72	35	20	2	2,5	0,67
Gear d_2	2	112	56	20	2	2,5	0,67

Bending verification

According to Spur Gears Theory [3] it must be respected the relation $\sigma_{eff} = \frac{F_t}{wmJ} K_v K_0 \leq \sigma_{amm} = C_1 C_2 \frac{\sigma_{C40}}{f}$.

If it's considered

- $F_t = \frac{2T}{d_1} = 333[N]$ tangential force
- $v_1 = \omega_1 \frac{d_1}{2} = 0,19 \frac{m}{s}$ linearity velocity
- Velocity factor $K_v = \frac{5,56 + \sqrt{0,19}}{5,56} = 1,08$ for ground gear
- Overload factor $K_0 = 0,8 = k_v$ it's equal to service factor
- Geometry factor $J = 0,28$ Lewis theory, where it's considered $z = 35$ interpolation, pressure angle $\alpha = 20$
- surface finish factor $C_1 = 0,85$ grinding process
- sizing factor $C_2 = 1$, considering $m < 5$
- $\sigma_{Y,C40} = 430 [MPa]$ hardened and tempered steel C40, safety factor $\Phi = 2$

Thus $\sigma_{eff} = \frac{F_t}{wmJ} K_v K_0 = 35,68 [Mpa] \leq \sigma_{amm} = C_1 C_2 \frac{\sigma_{C40}}{f} = 182 [Mpa]$, the spur gear is then verified for bending stress.

Wear verification

The equation of wear verification according to Spur Gears Theory [3] is $\sigma_H =$

$$0,59 \sqrt{\frac{F_t E (1 + \frac{d_1}{d_2})}{wsin(2\alpha)r_1}} K_v K_0 \leq \sigma_{H,amm} = 2,22 \cdot HB + 200$$

- hardened and tempered steel C40, $HB = 400 \div 600$, $E = 220 [GPa]$
- $\sigma_H = 0,59 \sqrt{\frac{F_t E (1 + \frac{d_1}{d_2})}{wsin(2\alpha)r_1}} K_v K_0 = 330 [MPa]$
- $\sigma_{H,amm} = 2,22 \cdot HB + 200 = 1310 [MPa]$

Spur gears are verified for wear stress.

5.2 Design and verification of the user shaft

The aim is to study the forces to find the minimum diameter. First of all, the forces acting on the shaft at each point are found, then the internal and external force equations are written to find the stresses. The computation of the equations was done with the Wolfram Mathematica software.

The below *Figure 14* shows the tensions exerted on the rope (black) and the net (green).

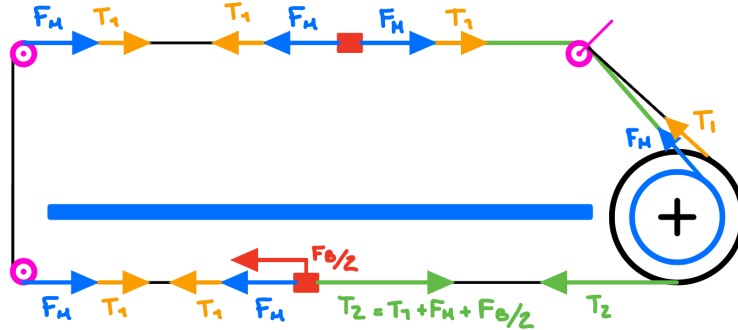


Figure 14: Forces scheme of rope and net

Data

Before designing the mechanical shaft, it is necessary to estimate the force transmitted by the gear wheel. To do this, the torque at point E was set as an unknown, and then the torque necessary to balance the system was calculated.

To know the friction, an experimental test would be required, so we decided to choose a slightly larger engine that would first be able to balance the system, then add the power necessary to overcome the friction.

So we do the force analysis with the point of the gear wheel as an unknown, it turn the Torque equal to $T = 6840,6 \text{ [Nm]}$, Thus $F_t = \frac{2T}{d_2} = 122 \text{ [N]}$ and $F_r = F_t \tan(\alpha) = 44 \text{ [N]}$.

Below, in *Figure 15* is reported the sketch scheme of shaft loads.

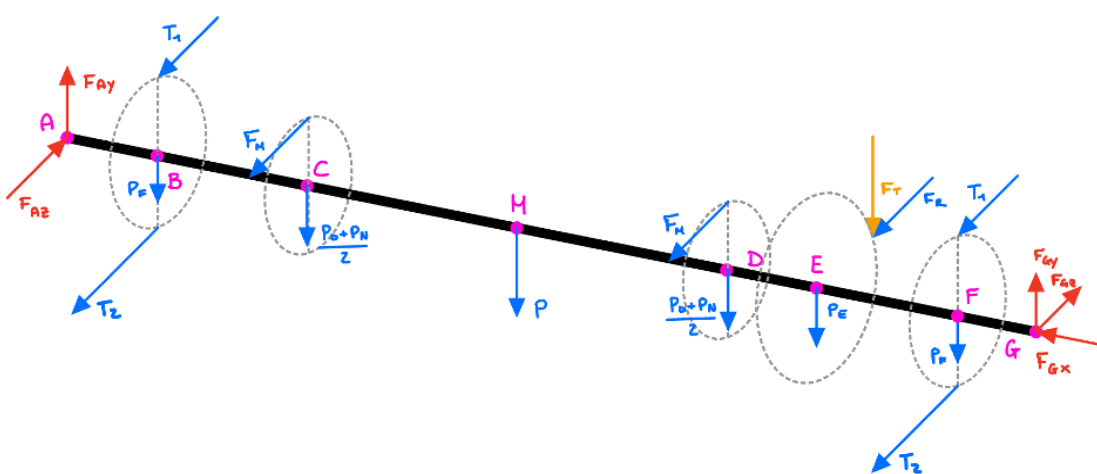


Figure 15: Scheme of shaft loads

The values of all the data chosen or calculated in the analyzes of the other chapters are also reported in the following *Table09*

Table09: Description and values of analysis force data

Data	Description	Values
Spring forces F_m	Value is defined from the net deflection analysis <u>cap01</u>	$F_m = 100 [N]$
Radial engine force F_r	Value is defined from the Torque necessary to ensure equilibrium	$F_r = 112 [N]$
Upper rope tension T_1	Rope pre-tensioning	$T_1 = 25 [N]$
Brush force F_b	Value is defined from the cleaning system design	$F_b = 150 [N]$
Lower rope tension T_2	Value is the sum of pre-tensioning, spring force, brush force	$T_2 = T_1 + F_m + \frac{F_b}{2} = 200 [N]$
Spur gear weight P_E	Assumed that it's made of steel	15,2 [N]
Net weight P_N	Value is defined from catalog	1,96 [N]
Drum net weight P_D	Assumed that it's made of aluminum	24,5 [N]
Drum rope weight P_F	Value is defined from catalog	6,4 [N]
Shaft weight P	Assumed that it's made of steel	69,4 [N]
Net rope radius r_1	Value is defined from the analysis <u>cap01</u>	40 [mm]
Drum rope radius r_2	Value is defined from the analysis <u>cap01</u>	42,4 [mm]
Spur gear radius r_t	Value is defined from the motor transmission analysis <u>cap01</u>	56 [mm]

The equations to determine the internal forces were written in Mathematica, which as output gives the following stresses for each point summarized in the *Table10*.

Table10: forces acting on the points of the shaft

Points	Length from constraint A	Forces					
		N	T_y	T_z	M_y	M_z	M_x

	[mm]	[N]	[N]	[N]	[Nmm]	[Nmm]	[Nmm]
A	0	0	-46	328	0	0	0
B	39	0	-38	103	-12500	1800	7400
C	88,5	0	-27	3	-17800	3600	3400
M	633,5	0	40	3	-19500	18300	3400
D	1173,5	0	51	-97	-21100	-3300	-580
E	1188,5	0	-56	-141	-20000	-4000	-7400
F	1228,5	0	-56	-366	-14200	-1800	0
G	1267	0	-56	-366	0	0	0

Minimum diameter

In order to design a shaft we need to consider stress factors, geometry and material properties. The following inequality takes into account all of them:

- $K_f \sigma_{eq} = \sigma_{eq,eff} \leq \sigma_{all} = \frac{\sigma_{cr,part}}{\phi} = \frac{C_s C_d C_{load} \sigma_{cr}}{\phi}$

At first we can calculate σ_{all} . It's considered hardened steel C40 UNI 7846, $\sigma_{Y,C40} = 430 [MPa]$, $\sigma_{UTS,C40} = 700 [MPa]$ and $\phi = 2$.

- Surface finish on a machined shaft is $C_s = a\sigma_R^b = 0,79$,
- Size coefficient it's equal to $C_{load} = 1$ since the shaft is subjected to bending and torsion,
- $C_d = 1,189d^{-0,097} = 0,89$ considering $d = 20 [mm]$
- So we have the result $\sigma_{all} = \frac{C_s C_d C_{load} \sigma_Y}{\phi} = 151 [MPa]$

Then it's important to know σ_{eq} for each section point.

- $M_{bending,tot} = \sqrt{M_y^2 + M_z^2}$
- $M_{bending,eq} = \sqrt{M_{f,tot}^2 + \alpha M_t^2}$, $\alpha = 0,25$ since the torque is assumed to be constant
- finally we can know $\sigma_{eq} = \frac{32M_{bending,eq}}{\pi d^3}$

We obtain the equation of $d_{min} \geq \sqrt[3]{\frac{32M_{bending,eq}K_f}{\pi\sigma_{all}}}$.

Some points present a notch factor, so it's important to take account of them, in order to have a table with the minimum shaft's values allowable.

Notch sensitivity is defined by the relation $K_f = 1 + q(K_t - 1)$

For the calculation of the notch factor, the iterations due to the unknown diameter will not be shown, will be considered only the final values of the shaft.

- Parallel key notch factor. Below is shown the computation for point B, for others points are reported values on table01
 - It's compute $\frac{r_f}{d} = 0,0125$ considering $d = 20 \text{ [mm]}$ and fillet radius $r_f = 0,25 \text{ [mm]}$ according to the UNI6604 reference standard.
 - Following charts of fatigue calculation $K_t = 2,9$ and $q = 0,81$, thus $K_f = 1 + q(K_t - 1) = 2,52$
- Shoulders notch factor. Only points A and G will be studied, given that the other shoulders do not correspond to any concentrated force and for this reason have not been studied analytically. Other shoulders are not close to the two most critical points (medium point M and spur gear point E), so there should be no critical issues. However, a FEM analysis will also be performed subsequently to ensure the correctness of the treatment.
 - Let's study points A and G, $\frac{D}{d} = 1,33$ considering $D = 20 \text{ [mm]}$ and $d = 15 \text{ [mm]}$. Thus $\frac{r_f}{d} = 0,03$ where $r_f = 0,4 \text{ [mm]}$.
 - Following charts of fatigue calculation $K_t = 2,5$, $q = 0,81$, thus $K_f = 1 + q(K_t - 1) = 2,22$

Values of notch factor and equivalent bending change for every point. So from the datasheet of stresses in *Table10* are obtain the values on the *Table11*:

Table11: Notch factors

Points	$M_{bending,eq}$	K_f	d_{min}
A	54	2,22	3,50
B	11600	2,52	12,90
C	17367	3,03	15,43
M	19220	/	12,18
D	22285	3,03	16,29
E	19500	2,52	15,14
F	13400	2,52	13,45
G	344	2,22	2,79

The most critical point for the diameter is point D. In the final design it's decided to oversize the shaft also to avoid deflections.

The *Figure16* shows a section of the final shaft, the technical table with the relevant measurements can be found on annexes.

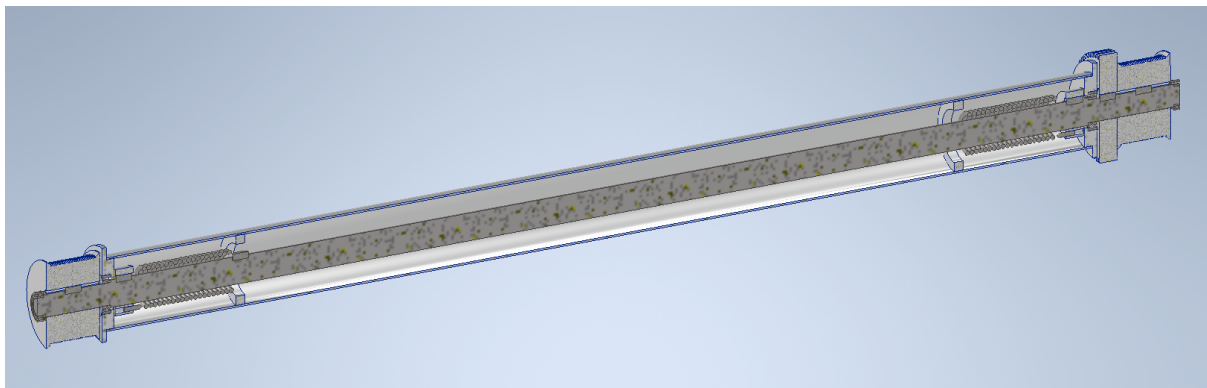


Figure 16: Section of final shaft design

FEM analysis

The FEM analysis was performed with Autodesk Inventor Nastran 2024, specific software for finite element analysis. The structure was meshed with 20 [mm] parabolic meshes and using a translational constraint along the y-z axis to simulate the axially free bearing and a translational constraint on all 3 axes on the other bearing, the one also axially constrained. The maximum forces of radial loads and moments were then applied to the component, which were simulated as forces applied on the lateral contact faces of the keys.

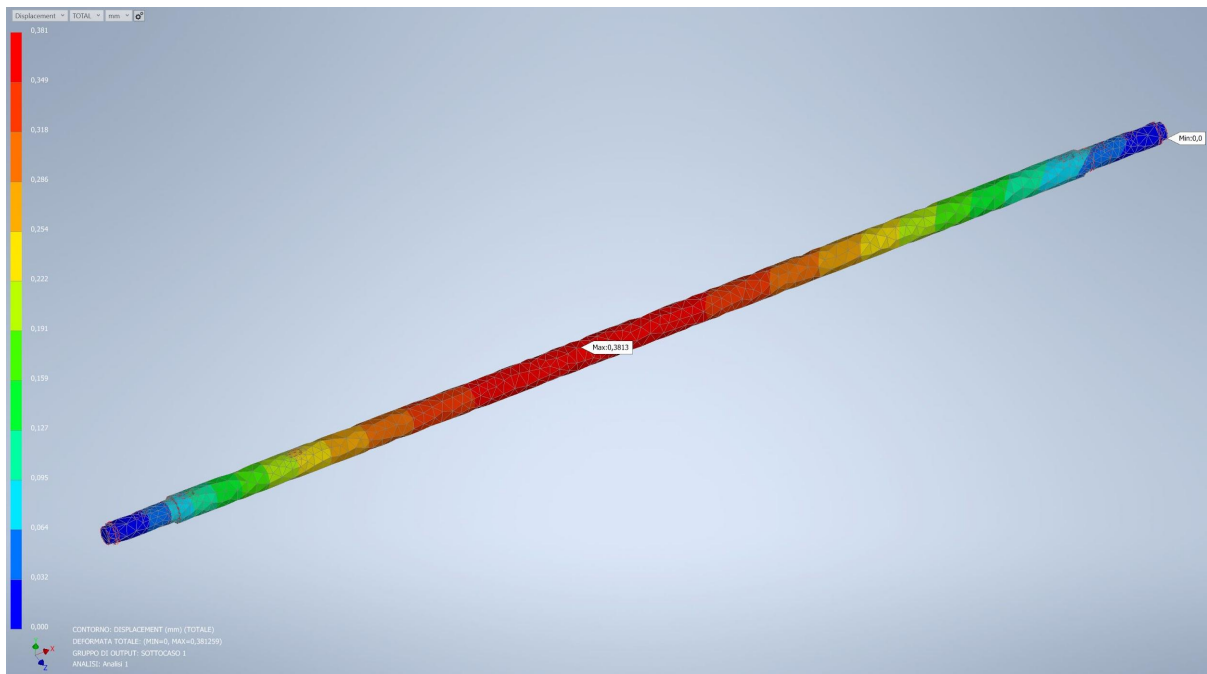


Figure 17: Shaft FEM analysis

Figure 17 shows the deformation modulus on all axes, displayed with real scale and with 12 discrete bands of color equally distributed from 0mm to the maximum deformation that occurs on the shaft, equal to 0,381 [mm]. Now we need to study stiffness on critical points:

- The transverse deflection allowed by a spur gear with module $1 < m < 3$ is $\delta_{all} = 0,075$ [mm]. From the FEM analysis it appears that at this point there is a deformation of $\delta_E = 0,073$ [mm].
- Deformation allowable of deep groove ball bearing, it must be less than $\theta_{all} = 0,003$ [rad]. The greatest deformation is on the bearing at point A, which has $\theta_A = 3,50 \cdot 10^4$ [rad].

Therefore, both conditions are verified $\delta_E \leq \delta_{all}$, $\theta_A \leq \theta_{all}$ and therefore the shaft is verified by stiffness.

5.3 Coupling design

Bearing verification

In the project we have neither large loads nor numerous usage cycles. The critical issue in our choice of bearings is the operating conditions. For this reason, a stainless-steel deep groove ball bearing with integral sealing was chosen.

Bearings with seals are preferred for arrangements where contamination is moderate. Where the presence of water or moisture cannot be ruled out, contact seals are typically used.

It also has greater chemical and corrosion resistance, Grease LHT23 is used. Now we limit to compute the verification of the from the bearings chosen in the Figure 18 from SKF catalog[2].

Bearing Properties		W 61804-2RZ								
SKF		Bearing type	Principal dimensions			Basic load ratings			Speed ratings	
Designation		Bore	Outer diameter	Width	Dynamic	Static	Fatigue load limit	Reference	Limiting	
		d (mm)	D (mm)	B (mm)	C (kN)	C ₀ (kN)	P _u (kN)	n _{ref} (r/min)	n _{lim} (r/min)	
W 61804-2RZ	Deep groove ball bearing	20	32	7	3.12	2.08	0.09	48000	24000	

Figure 18 Characteristics of the selected bearing

- $h_{tot} = n_{days}n_{months}n_{years}n_c = 3600$ [cycles] considering a use of 15 days per month for the no-maintenance period declared in the specifications (10 years). It is also considered that each operation is followed by two different cycles (forward/return), which is why it has been multiplied by a factor n_c .
- The number of cycles corresponding to the requested life is $N = h_{tot}\omega_2 60 = 1,134 \cdot 10^5$ [cycles] thus $L_1 = 0,13$

- $F_{G,R} = \sqrt{F_{Gy}^2 + F_{Gz}^2} = 34$ [N], $F_A = 0$, thus $Y = 0$
- $F_{G,R,eq} = F_{G,R} = 34$ [N]
- $L_2 = \left(\frac{C}{F_{R,eq}}\right)^3 a_1 a_{SFK}$
- Reliability of 95% is enough, thus $a_1 = 0,64$
- operating temperature is assumed 50°C because of sunning days on the roof
- from SKF catalog, by interpolating it's obtain Grease LHT23, $v = 26$ [$\frac{mm^2}{s}$]

- High cleanliness condition for sealing bearing that are greased for life $\eta_c = 0,6$.
- $n_2 = 31 \frac{rev}{min}$, $d_m = 26 [mm]$ thus rated viscosity is $\nu = 420 \frac{mm^2}{s}$
- viscosity ratio it must be $K = \frac{\nu}{\nu_1} = 0,06$, $\eta_c \frac{P_u}{F_{G,R,eq}} = 2,64$ thus $a_{SFK} = 0,1$
- $L_1 = (\frac{C}{F_{G,R,eq}})^3 a_1 a_{SFK}$ if it's arrange $C = F_{G,R,eq} \sqrt[3]{\frac{L_1}{a_1 a_{SFK}}} = 43 [N]$, $C_{all} = 4000 [N]$

Therefore, as expected, the bearings were tested with a large gap compared to the critical condition. The bearings will be interference mounted as per SKF specifications, the details are represented in the annexed technical drawing.

Parallel keys

Shaft diameter at keyseat determines the key width. The dimensions will be found according to the UNI6604 reference standard, and then a verification of the forces will be carried out.

The forces of the analyzes are small, which is why all the same tabs were chosen and in the case of C and D the minimum length recommended for the diameter of those points, the dimensions are shown in the below *Table12*.

Table12: Parallel key and keyseat dimensions according to UNI6604 reference standard

	Parallel key				Keyseat			
	Shaft diameter	Section	Lenght	Key chamfer	depth in the shaft	depth in the hub	toleranc e	fillet radius
	d_2	$b \times h$	L	s	t_1	t_2	$t_1 - t_2$	r
	[mm]	[mm]	[mm]	[mm]	[mm]	[mm]	[mm]	[mm]
B,E,F	25	8×7	18	0,40	4	3,3	0,2	0,25
C,D	30	8×7	18	0,40	4	3,3	0,2	0,25

As far as verification goes, they were chosen key material C20 steel, thus $\tau_{all} = 50 \text{ [MPa]}$, $\sigma_{all} = 100 \text{ [MPa]}$, verification values are shown in *Table13*.

Table13: Parallel keys verification

Verification	Torque	σ verification	τ verification
	T	$\sigma = \frac{2T}{(h - t_1)Ld} \leq \sigma_{all}$	$\tau = \frac{2T}{dbL} \leq \tau_{all}$
B, E, F	7400 [Nmm]	$10,96 \leq \sigma_{all}$	$4,11 \leq \tau_{all}$
C	3400	$4,19 \leq \sigma_{all}$	$1,57 \leq \tau_{all}$
D	580	$0,72 \leq \sigma_{all}$	$0,26 \leq \tau_{all}$

All the parallel keys are verified.

5.4 Rod rope support

The size of the rod that supports the transmission cable pulleys must be slim and have a reduced anchoring base. The first characteristic derives from the need to create as little shadow as possible on the panel, the second from taking up little space for anchoring on the roof.

Section design

From the analysis of the forces, the most stressed areas appear to be near A and B.

A catalog pulley with a diameter $d = 6 \text{ [mm]}$ was chosen, the total height of the rod is $H = 375 \text{ [mm]}$ to ensure a distance between the net and the panel of 3000 [mm] as per specifications, a scheme of the stick is summarized in *Figure01*

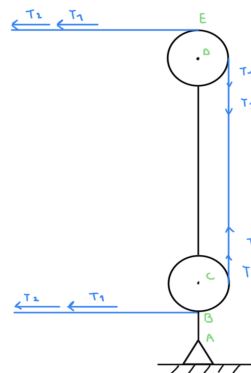


Figure19: Load rope support scheme

From the analysis of the forces, the most critical points are A and B, the forces in these points are schematized in the *Table 14*.

Table 14: Rod greater stresses

	Greater stresses	A	C
	M_b	53125 [MPa]	46875 [MPa]
	V	250 [N]	125 [N]

Now we want to calculate the ideal sections on the rod in points A and C, where there is the hole due to the pulley as shown in *Figure 20*.

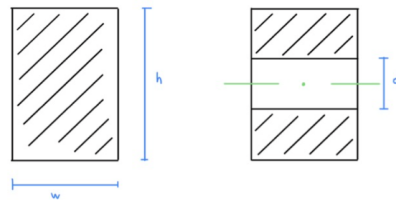


Figure 20: Section of point A (left) and point C (right)

- By setting a reasonable value of $w = 10\text{mm}$, by rearranging terms od $\sigma_A = \frac{M_{b,A}h}{2I_A} \leq \frac{\sigma_{Y,C40}}{\phi}$, we find that $h_{min,A} \geq \sqrt{\frac{\Phi M_{b,A}}{\sigma_{Y,C40}w}} = 9,6 [\text{mm}]$. Where are considered $\Phi = 1,25$ static case, hardened steel C40 UNI 7846, $\sigma_{Y,C40} = 430 [\text{MPa}]$.
- As regards section C, the equation $\sigma_B = \frac{M_{b,C}h}{2I_B} \leq \frac{\sigma_{Y,C40}}{\phi}$ leads to $\frac{6M_{b,C}h}{w(h^3-d^3)} \leq \frac{\sigma_{Y,C40}}{\phi}$ where $d = 6[\text{mm}]$ is the pulley hole's diameter. Given the third degree inequality, it is preferable to proceed by iteration, after some attempts the values were obtained $h_C = 15 [\text{mm}]$, $w_C = 10[\text{mm}]$, it's verified $\sigma_B = \frac{6M_{b,C}h}{w(h^3-d^3)} = 133 [\text{MPa}] \leq \frac{\sigma_{Y,C40}}{\phi} = 286 [\text{MPa}]$.

In the sizing of section C, notching effects were not considered since in the static case they are compensated by microplasticization phenomena.

In conclusion the most critical section is C, which is why the measurements are chosen the values $h = 15[\text{mm}]$ and $w = 10[\text{mm}]$.

Welded joint

A Fillet Joint was chosen as the efforts are static and limited, the sketches are shown in *Figure21*.

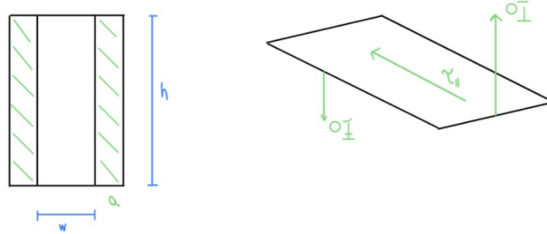


Figure21: Geometry and Load scheme of welding section

- By the Truncate Sphere Criterion the equation is $\sqrt{\sigma_{\perp}^2 + \tau_{\parallel}^2} = \nu \sigma_{all}$ where it's considered $\sigma_{all} = 160 \left[\frac{N}{mm^2} \right]$ and $\nu_1 = 0,7$.
 - A reasonable value is estimated on $a = 3 [mm]$, thus throat height is $t = a \frac{\sqrt{2}}{2} = 2,12 [mm]$.
 - thanks to the beam theory we obtain the values of σ_{\perp} and τ_{\parallel} :
 - $\sigma_{\perp} = \frac{M_A}{I} \cdot \frac{h}{2} = \frac{6M_A}{h^2} = 22,96 [MPa]$
- $$\tau_{\parallel} = \frac{V}{2ht} = 2,77 [MPa]$$

Developing the Truncate Sphere Criterion it's verified the condition $\sqrt{\sigma_{\perp}^2 + \tau_{\parallel}^2} = 23,12 [MPa] \leq \nu \sigma_{all} = 112 [MPa]$, thus safety margin is $f = \frac{112}{23,12} = 4,84$

Bolted joint verification

For brevity, the iterations that led to the size of the joint are not reported, in this paper is only proposing a solution to verify it. Screw arrangement schem is shown in *Figure22*.

Assumption:

- all the bolts are in tension
- $\Phi_{tension} = \Phi_{shear} = 1,25$ below static condition
- Number of screws $n_b = 4$

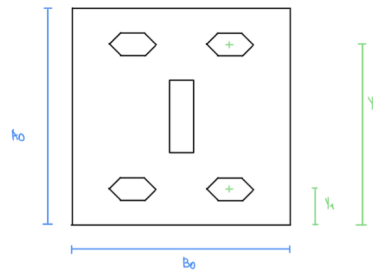


Figure22: Screws arrangement scheme

Screw datasheet is summarized on *Table15*.

Table15: M5 Screws datasheet

Screw datasheet	Bolt class	Head diameter [mm]	Resistant area [mm]	Tension allowable [$\sigma_{all,N}$]	Shear allowable [$\sigma_{all,T}$]
METRIC SCREW UNI EN ISO 7046 M5	4,8	9,3	14,2	187	132

- Under hypothesis of rigid members/compliant bolts, shearing force is equally distributed among the bolts $V_{i,A} = \frac{V_A}{n_b} = 62,5 [N]$
- Now the aim is determinate the most critical value of N_b .
 - From the relation $M_x = \sum_i C' y_i^2$, rearranging terms it's obtain the constant value $C' = \frac{M_x}{2y_1^2+2y_2^2} = 5,53 \frac{N}{mm}$.
 - To reach the value of y_n it's used the relation $\sigma_{max,co} \frac{y_n^2}{2} B_0 + \sigma_{max,co} A_b [2(y_n - y_2) + 2(y_n - y_1)] = 0$, solving the quadratic equation $y_n = 8,85 [mm]$.
 - In order to determinate value of $\sigma_{max,co}$, It's solve the equilibrium equation $B_0 \frac{\sigma_{max,co} y_n^3}{3} + \sigma_{max,co} A_b [2(y_1 - y_n)^2 + 2(y_2 - y_n)^2] = M_x y_n$ thus $\sigma_{max,co} = 6,30 [MPa]$
 - Finally form previous result, the stress values are known
 - $\sigma_1 = -\sigma_{max,co} \left(1 - \frac{y_1}{y_n}\right) = 0,82 [MPa]$,
 - $\sigma_2 = -\sigma_{max,co} \left(1 - \frac{y_2}{y_n}\right) = 29,23 [MPa]$
- N_{b2} is negligible, so It's considered $N_{b1} = \sigma_2 A_b = 415 [N]$.

Let's now check whether the values found verify the resistance conditions of the materials; all the properties of the screws are shown in the *Table15*.

Are thus verified the inequalities:

- $N_{b1} = 415 [N] \leq \frac{\sigma_{amm,N} A_{bt}}{\phi_{tension}} = 2124 [N]$
- $V_{i,A} = 62,5 [N] \leq \frac{0,58 \sigma_{amm,T} A_{bt}}{\phi_{shear}} = 870 [N]$

5.5 The cleaning system

In the following section the cleaning mechanism and its components will be chosen and dimensioned step by step.

Nylon roller/rotating brush

In order to clean the panel a rolling nylon brush was selected. It was discovered that this type of brush is commonly realized to measure by the supplier and the dimensions needed to fit our application are easily found, since it's one of the most used brushes for cleaning solar panels and it's commonly sold precisely for this application.

The selected brush [5] is visible in *Figure23*.



Figure23: Picture of the selected rotary brush

On *Table16* the brush datasheet is summarized.

Table16: Datasheet of the selected brush

Color	white, black, yellow
Size	Custom brush size (for a length of 1000-2000mm a diameter of 150mm is commonly used) Aluminum alloy tube: 20mm inner diameter 25mm outer diameter 2.5mm thickness
	Plastic tube 25mm inner diameter 43mm / 52mm outer diameter
Material	Bristle: Nylon, PBT Bristle thickness: 0,25mm or customized Tube: Plastic tube and aluminum alloy tube

As previously introduced in the chapter concerning the development of the project and its subunits, given the impossibility to analytically model the brush, similar commercial applications and papers that discuss solar panel cleaning were studied to obtain the values of the most important characteristics of the rotating brush cleaning system:

- The brush should rotate between 60 and 200 RPM
- The torque needed to rotate the brush should be at maximum 3 Nm 3 [Nm]

Given the chosen brush, the estimated weight of the brush and its aluminum shaft is 3 kg, and the hollow shaft has the following characteristics:

- External Ø 25 mm
- Internal Ø 20 mm

From the study of similar commercial applications it was established that the brush should be pressed towards the panel with a relatively small force of around 150 N to achieve an effective cleaning, so a mechanism to retain the brush against the panel will be needed.

Force analysis

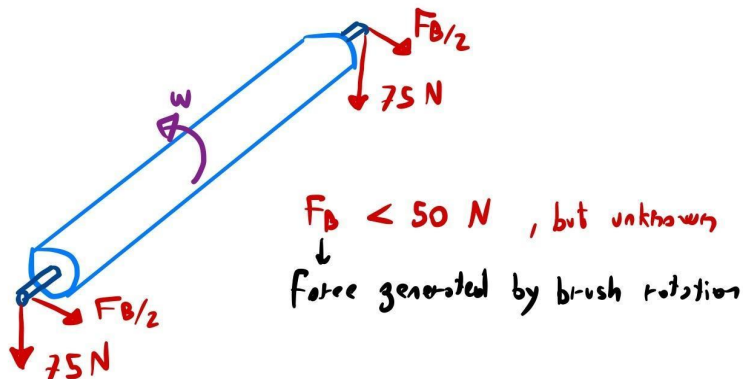


Figure24: Forces exerted on the rotating brush

Through an analysis of similar applications it was discovered that for an effective cleaning the brush needs to be pressed against the panel with a force of 75 [N] per side (150 [N] total). While the brush rotates the force it generates through its rotation F_B cannot be analytically calculated, but is estimated to be less than 50 [N] through a study on similar applications (see Figure24).

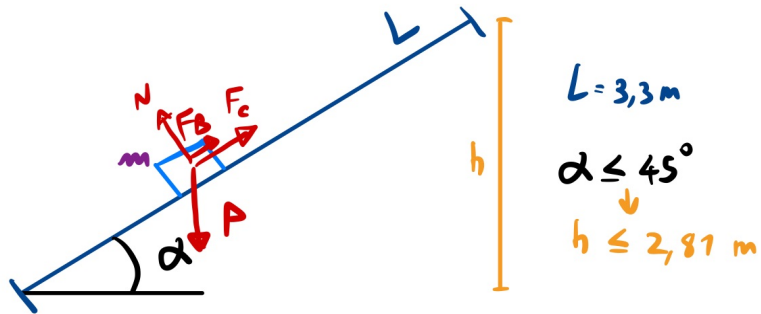


Figure 25: analysis of the equilibrium of the cleaning system on an inclined solar panel

The carrier system needs to be moved along an inclined solar panel (see Figure 25) with total length $L = 3,3\text{m}$.

The inclination of solar panels varies, but for the purpose of this analysis the worst case is assumed, so the maximum possible inclination of $\alpha = 45^\circ$ is used.

The weight of the carrier system is estimated as follows:

$$m = m_{brush} + m_{motor} + m_{wheels} + m_{cover} + m_{structure} = 3 + 0,5 + 1 + 5 + 10 = 20 [\text{kg}]$$

If the brush is rotated in the direction of the upward motion, the force F_B "helps" in sustaining the mass of the carrier, so as a worst possible case, for the purpose of this analysis, we assumed $F_B = 0$.

The force F_C that is needed to keep the carrier in position along the panel is then estimated as follows:

$$F_C = P \sin(\alpha) = 142 [\text{N}]$$

The force of the friction of the bearings that will be used in the wheels of the carrier is added: The loads on the wheels are negligible compared to what the bearings are rated for, so for the calculations of the friction they are overestimated:

For all the wheels a load of 100N is used, that with a rotation speed of 36 RPM gives a friction of 1.15 [Nmm], so the force exerted at the end of the wheel will be 0,03 [N].

A total of 6 wheels are present so the friction is 0,18 [N].

Since other possible frictions are not estimated, this value is increased for safety reasons and the total force needed to keep the carrier in position is estimated to be: $F_C = 146 [\text{N}]$

The power needed to move the cleaning mechanism is calculated when the main electric motor is dimensioned, and the contributions of the cleaning system were added in the calculation.

Brush rotation electric motor

Given the characteristics needed to actuate the rotation of the brush of the cleaning system, a planetary gear 24 V motor [10] with the characteristics shown in *Table 17* was selected:

Table 17: Datasheet of the selected planetary gear electric motor

Motor Datasheet	Nominal tension	L	Reduction ratio to :1	Nominal torque	No load speed
	[V]	[mm]		[Ncm]	[rpm]
P205 -24-39	24	133	39,06	350	105
No load current	Nominal torque current		Input power at nominal torque		Nominal torque speed
[A]	[A]		[W]		[rpm]
<0,4	2,10		20,2		77

The electric motor dimensions are as depicted in *Figure 26*:

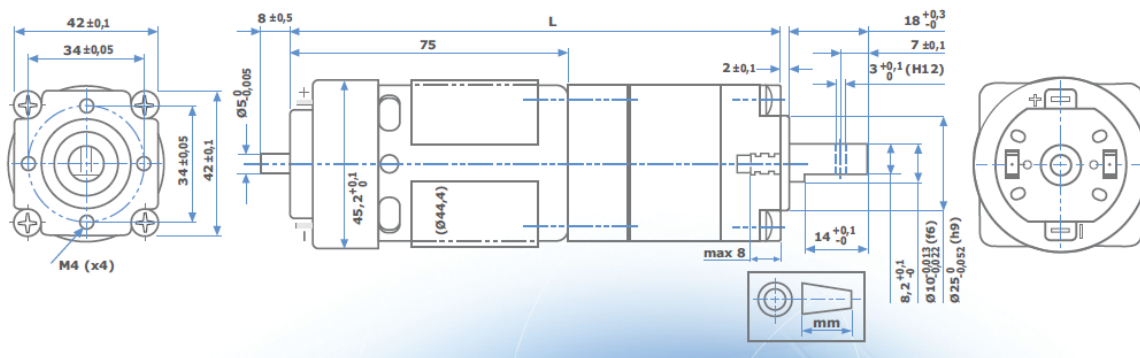


Figure 26: Dimensions of the selected electric motor

The brush will always be rotated in the direction of upward motion of the carrier to not generate a force that is going to sum to the weight of the carrier assembly and so the required torque and power for the movement of the cart is drastically reduced.

During the rotation of the brush some vibrations will be generated, so some kind of vibrational isolation between the brush and the motor will be needed.

The motor will be coupled to the brush through the use of a flexible oldham coupling [11] that provides vibrational isolation and misalignment compensation. The allowable torque of the joint should be over 3,5 [Nm] and the diameter of the holes has to be 10 [mm]. It should resist rotation speeds over 105 [RPM]. The selected coupling is shown in *Figure27* and its datasheet is presented in *Table18*.



Figure27: The selected oldham coupling for connecting the motor to the brush

Table18: Datasheet of the selected oldham coupling

Type	Oldham Type	Allowable Misalignment	Angular Misalignment / Eccentricity
Application	Standard	Allowable Torque Range(N•m)	5.01 to 10.00
Standard Hole Diameter d1(mm)	10	Standard Hole Diameter d2(mm)	10
Outer Diameter D(mm)	26	Overall Length L(mm)	25.6
Max. Rotational Speed Range(r/min)	4,001 to 10,000	Feature	High torsional rigidity / High durability / Backlash 0 / Vibration Absorption / Small
Body Material	Stainless Steel	Category	Coupling body

To join the oldham coupling to the brush a custom made coupling will need to be machined, as shown in *Figure28*.

This coupling will be inserted in the oldham coupling on one side, and contain the shaft of the brush on the other side, so the diameter of the shaft on one side needs to be 10 [mm], and the diameter of the hole on the other side needs to be 25 [mm].

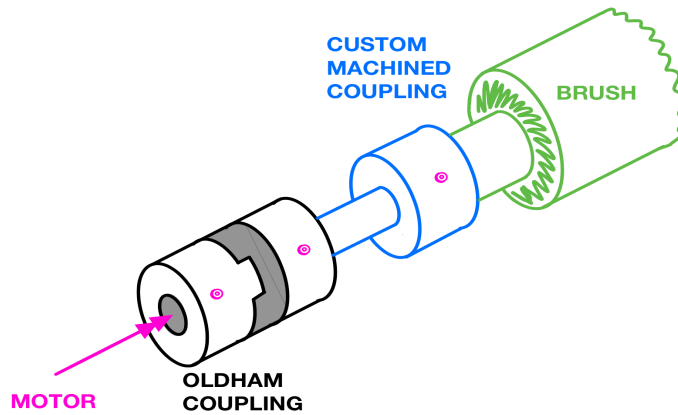


Figure28: Schematic drawing of the coupling between the electric motor and the rotary brush for the cleaning system

Bearing selection

The bearings for the brush have been selected from SKF catalog [2].

First we estimate the number of activations of the cleaning mechanism for the whole 10 years of no-maintenance period declared in the specification (the factor n_c represents the number of activations per “cycle”, as the whole mechanism needs to go back to the starting position after the activation). As a very conservative estimate of the number of activations we suppose to clean the panel every time the net needs to be extended, estimated to be 15 times a month:

- $n^\circ = n_{days} n_{months} n_{years} n_c = 3600 [\text{activations}]$

Then we estimate the number of cycles this corresponds to. Supposing a working time of 5 minutes every activation at 200 RPM, we get:

- $N = n^\circ * 5 * 200 = 3,6 \cdot 10^6 [\text{cycles}]$

SKF	Bearing type	Principal dimensions			Basic load ratings			Speed ratings		
		Designation	Bore	Outer diameter	Width	Dynamic	Static	Fatigue load limit	Limiting	
			d (mm)	D (mm)	B (mm)	C (kN)	C ₀ (kN)			
		W 61805-2RS1	Deep groove ball bearing	25	37	7	3.38	2.5	0.108	11000

Figure29: Characteristic of selected bearing

Verification is briefly reported, taking into account specification shown in *Figure29*. Given the conditions of liquids and dust with which they will come into contact, also in this case sealed bearings have been selected.

- $F_{eq} = \sqrt{F_y^2 + F_x^2} = 123 [N]$, where $F_y = 100[N]$, $F_x = 73[N]$. $F_A = 0$, thus $Y = 0$
- Assumed similar operating condition to shaft's bearings, the verification lead to the values $a_1 = 0,64$, $a_{SFK} = 0,6$.
- Thus $C = F_{eq} \sqrt[3]{\frac{L_1}{a_1 a_{SFK}}} = 259 \leq 3380 [N] = C_{all}$

The bearings of the cleaning system are verified.

The bearings are inserted in the transmission mechanism of the cleaning subunit as shown in *Figure30*.

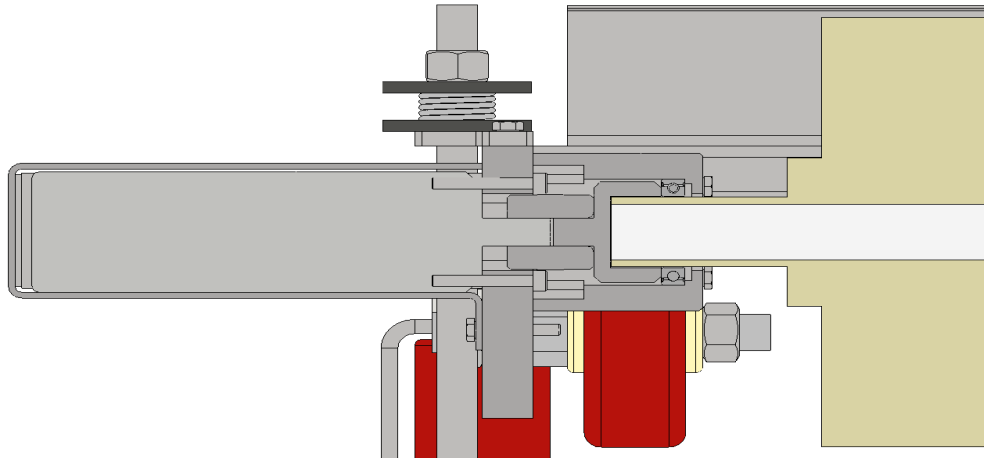


Figure30: Sketch of the relative positions of the various components of the cleaning system transmission. In order from left to right: electric motor, spacer, oldham coupling, custom machined coupling, deep groove ball bearing.

Carrier movement constraining

To constrain the motion of the carrier cart along the solar panel it was decided to use a set of polyurethane nylon roller bearing wheels as they are cheap but carry more than enough load, as the maximum load on a single wheel will be around 50 - 100 [N] but the maximum load capacity of a single wheel is 1200 [N].

These wheels will roll directly along the aluminum frame of the solar panel, and they will be adjusted in height to be able to be mounted on panels of different thicknesses thanks to a regulating mechanism present on the carrier cart.

The polyurethane nylon material is also abrasion resistant and resistant to water immersion, so the atmospheric conditions in which the system will operate will not be a problem.

These wheels can operate from -20 to +60 [°C] which is inside the nominal operating temperature for our application.

The dimensions of the selected wheels [12] are displayed in *Figure31*.

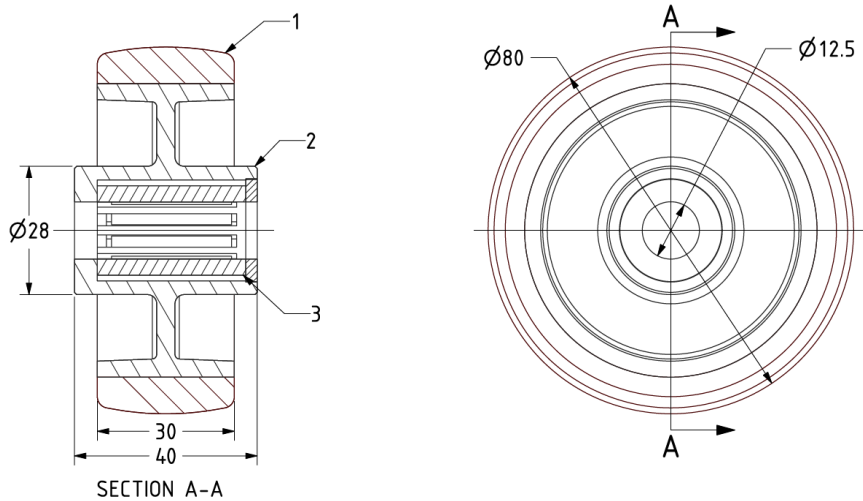


Figure31: Dimensions of the selected polyurethane nylon roller bearing wheels

The datasheet of the wheels is shown in *Figure32*.

**Polyurethane Nylon 80mm Roller Bearing Wheel
120kg Load**

Product code: BZMM80WPNRB

Brown polyurethane tyre on white nylon centred wheel with roller bearing. Diameter 80mm, tread width 30mm, bore size 12mm hub length 40mm Load capacity 120kg.



Bearing Type	Roller
Bore Size (mm)	12
Diameter (mm)	80
Hub Width (mm)	40
Load Capacity (kg)	120
Tread (mm)	30
Wheel Material	Polyurethane on Nylon
Colour / Shore Hardness	Brown Polyurethane on Nylon Rim / 96 Shore A
Temperature Resistance	-20 °C TO +60 °C

Figure32: Datasheet of the selected polyurethane nylon roller bearing wheels

The supplier of the wheels also sells custom made axles (*Figure33*) to fit the wheel and the necessities of the customer, so there is no need to create a shaft for the wheels from scratch.

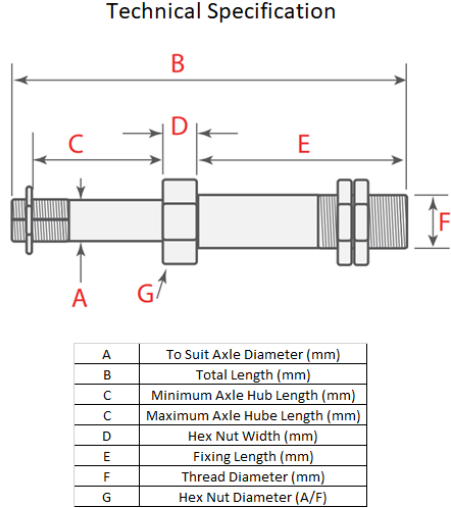


Figure33: Schematic drawing of the shaft to be used in combination with the selected polyurethane nylon roller bearing wheels

Another set of wheels [14] will be needed to constrain the motion of the cart along the panels and prevent derailment in extreme cases. These wheels do not have to support any load so they can be extremely small if needed.

The characteristics of the chosen roller are shown in *Figure34*, the model chosen is 231/150:

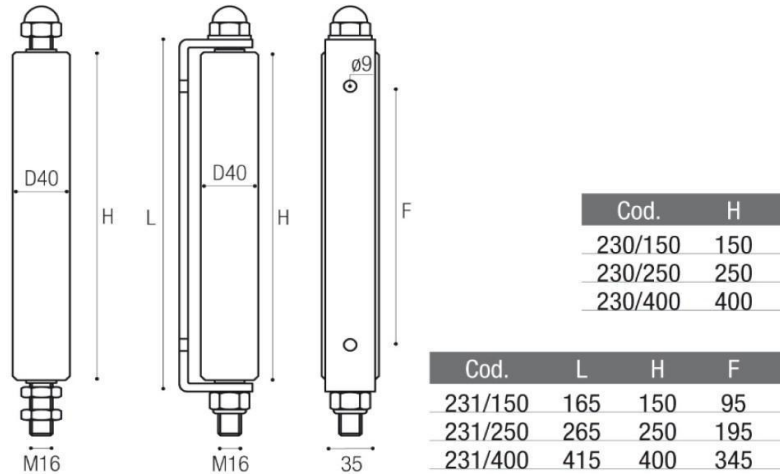


Figure34: Characteristics of the chosen rollers (model 231/150)

Steel cable connection

To connect the carrier to the steel cable that transmits its motion along the solar panel it was decided to use simple commercially available wire rope clips/steel rope clamps, which can be found in many sizes depending on the diameter of the cable (in our case 1,5mm) and can be directly attached to the side of the carrier cart. The general structure of a standard wire rope clip is shown in *Figure35*.

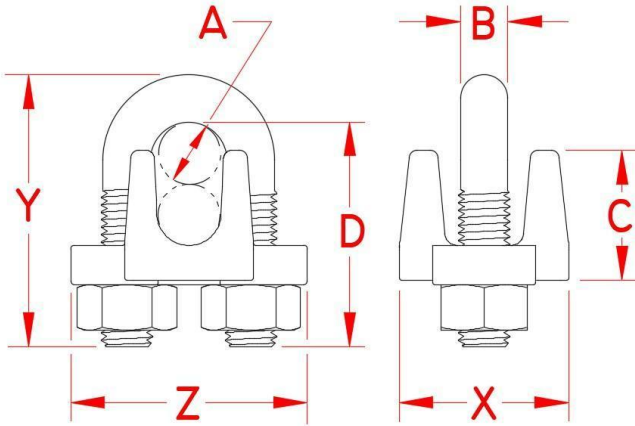


Figure35: Structure of a standard wire rope clip. Many different suppliers sell this kind of clip and the geometry is the same for almost all of them

Power connection

To connect the electric motor to electric power some kind of flexible power transmission is needed, as the cart with the motor moves along the solar panel.

To achieve this requirement it was decided to utilize an energy chain, as it is a readily available standard commercial solution to grant the mobility of cables along an axis. The energy chain has been chosen from the catalog [15] and is shown in *Figure36*.

Since only one power cable has to be moved, a chain which can accommodate a cable with a Ø of 7mm was selected.

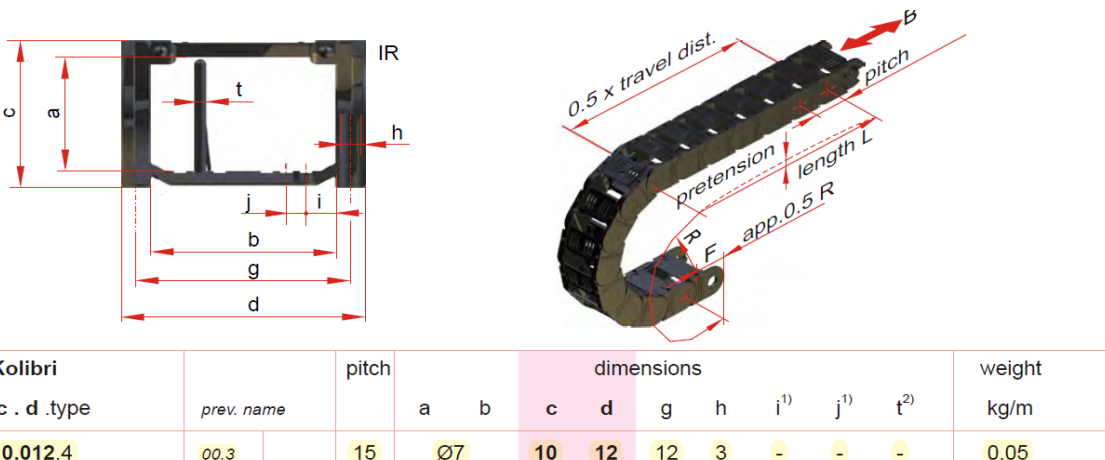


Figure36: Dimensions of the selected energy chain.

This energy chain will need a rail to ride along, so an aluminum rail will need to be installed under the solar panel or next to it, depending on the available space, in which the energy chain will ride.

$$\text{The length of the energy chain will be } L = \frac{\text{travel distance}}{2} = \frac{3,3 \text{ [m]}}{2} = 1,65 \text{ [m]}$$

Spring for brush contact

To ensure a constant contact between the brush and the panel with a force of 150 [N] (75 [N] per side), a helicoidal spring is used to tension the upper part of the carrier system with the brush to the lower part, fixed in respect to the panel (see *Figure37*).

The use of a spring has the added benefit of compensating for the brush wear as the rotating brush gets used to clean the surface of the panel, as a reduction on the brush diameter is compensated by an elongation of the spring.

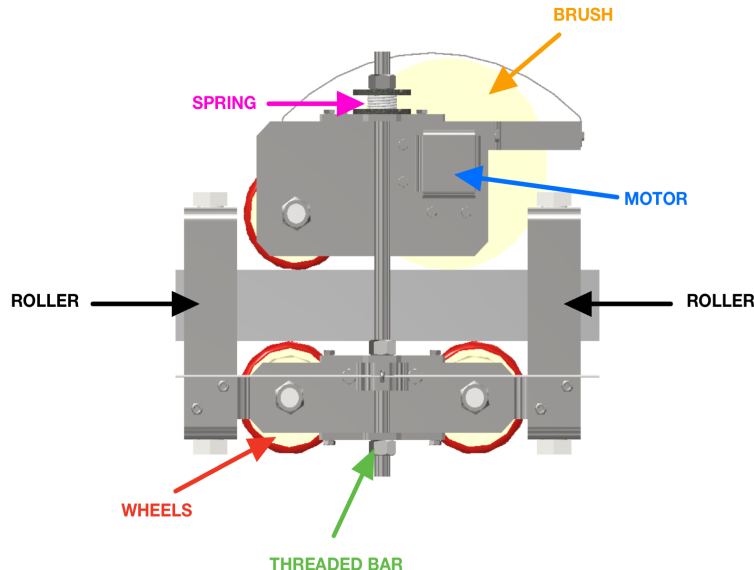
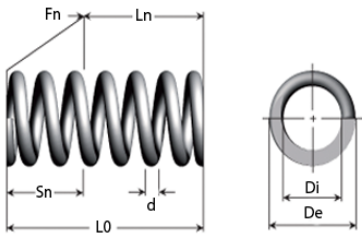


Figure37: Structure of the cleaning system. The division in two different carts, one riding over the panel and one under the panel is visible. The connection of the two carts through a spring loaded threaded bar is shown.

The chosen spring [13] is going to be mounted around an M12 threaded bar, and due to its position in the carrier mechanism has to output 120 [N] of force when compressed. The characteristics of the selected spring are presented in *Figure38*.



Materiale	Acciaio inossidabile 302
d - Diametro filo (mm)	2.67
De - Diametro esterno (mm)	24.77
Di - Diametro interno (mm)	19.43
L0 - Lunghezza senza carico (mm)	38.10
Ln - Lunghezza con carico max. (mm)	24.87
Sn - Corsa massima (mm)	13.23
Fn - Carico massimo in a Ln (N)	119.28
R - Costante della molla (N/mm)	9.01
Gamma	B

Figure38: Characteristics of the selected spring provided by the supplier

Carrier assembly

The structure to contain all the elements of the cleaning system has been defined as in Figure39.

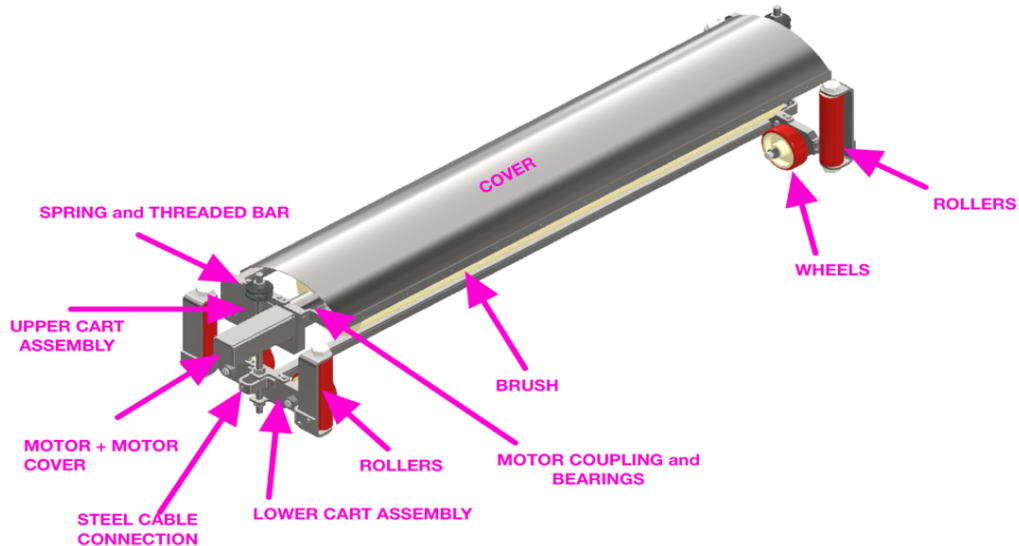


Figure39: Final design of the cleaning system. The main components have been highlighted and marked.

The cleaning unit is parked on the frame of the solar panel when not in use, in the opposite end of the panel in relation to the net deployment subunit. It is noted that if needed a structure for prolonging the frame of the solar panel (some aluminum extrusions bolted at the end of the panel) can be installed, so the cleaning system is stationed outside the surface of the panel and does not obstruct the sunlight.

6 PROJECT REVIEW

During the design process, primary importance was given to the effectiveness of the mechanism, understood as the ability to comply with all the project specifications.

The cleaning and protection system for solar panels is a complex mechanism with numerous pieces. Although this is actually to be expected given the innovative nature of the project. In fact, the mechanism for relaxing and winding the net was innovatively designed, and several difficulties had to be overcome compared to roller shutters with rigid rods.

The great advantage of the net is that it has very little impact on energy production: both because the roller box is smaller and because even when it is extended the panel can produce energy.

Among the major negative aspects we found:

- The actual effectiveness of the hail detection mechanism. An interesting development could be a mechanism that does not rely only on real-time hail detection but takes into account weather forecasts and warnings.
- Installation on any panel. Unfortunately a compromise had to be found between the protection and cleaning capacity compared to the ease of installation of the system. Recessed panels (a minority compared to those mounted on aluminum structures) do not adapt well to the cleaning system.

On the other hand, the positive aspects are:

- The high protection of the panels and the closing speed of the mechanism. The system involving the ropes and the drum ensures a suitable height of the net, and speed of deployment.
- The use of the power of the single motor to combine the lifting of the cleaning brush and the stretching of the net. An innovative solution that allows the simplification of the transmission of the motion.
- Every single component was designed to require no maintenance during the period established in the specification. From the sealed bearings, to the HDPE net, to the choice of the cable the maintenance was taken into consideration.

It is noted that the resistance to water droplets and dust of the whole system can be implemented through the use of well fitted covers and gaskets on the most critical components (electric motors, transmission, couplings, bearings).

7 CONCLUSION AND ANNEXES

The group is proud to have designed this system that could help mitigate the effects of climate change on solar energy production.

While acknowledging its flaws, all critical components have been verified, for the sake of brevity in this report only the most important design processes have been reported.

Below there is the final CAD drawing *Figure37* and some details (*Figure38*, *Figure39*) of the system assembly followed by the technical table of the shaft *Figure40*

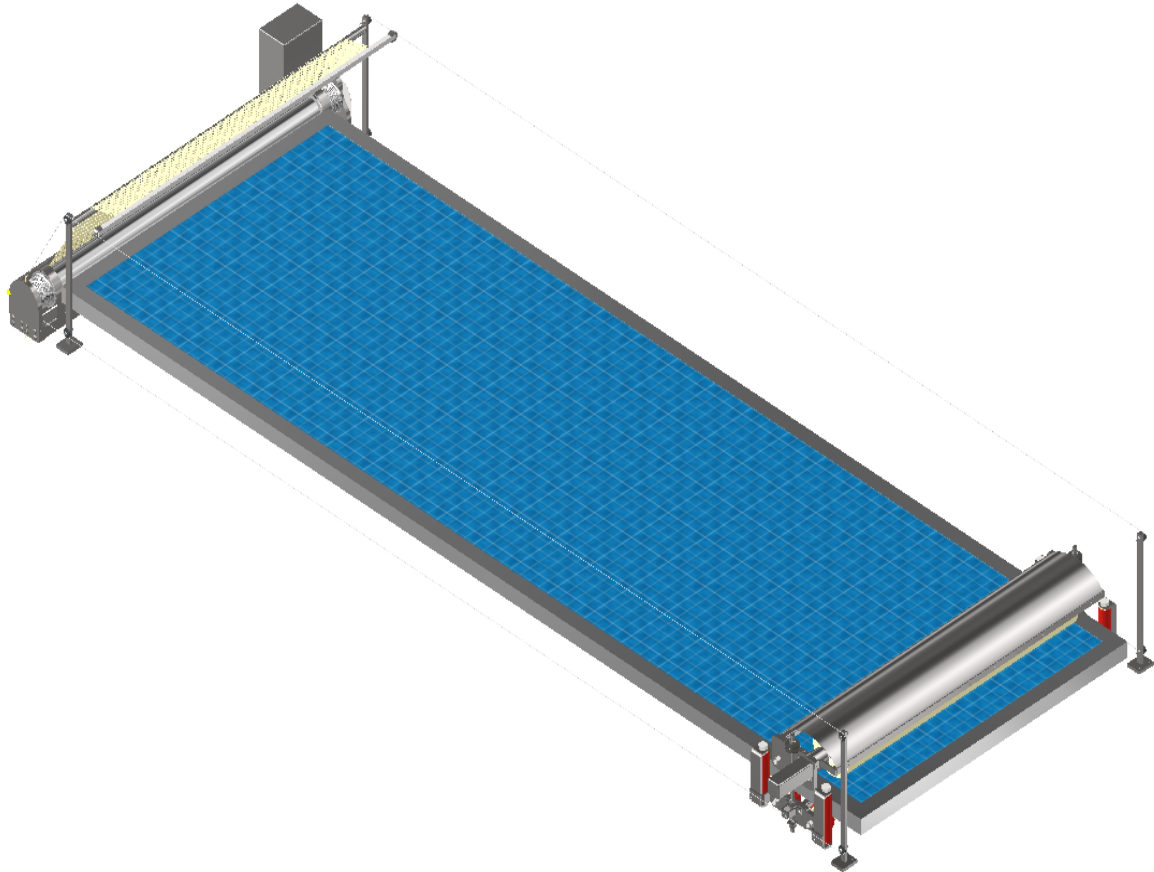


Figure37: 3D drawing of the final assembly

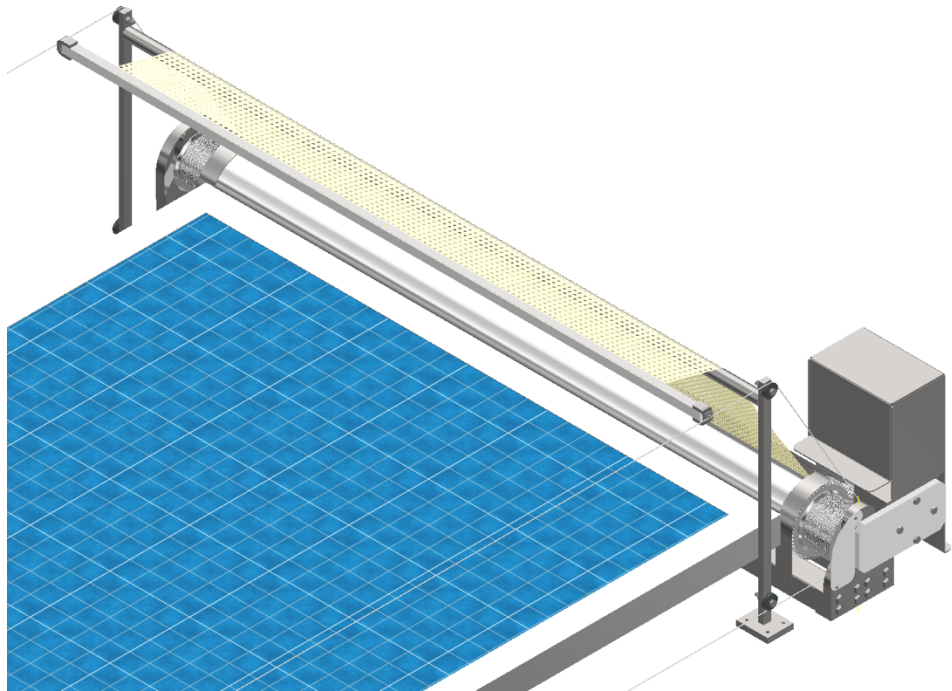


Figure38: Detail of the net deployment system

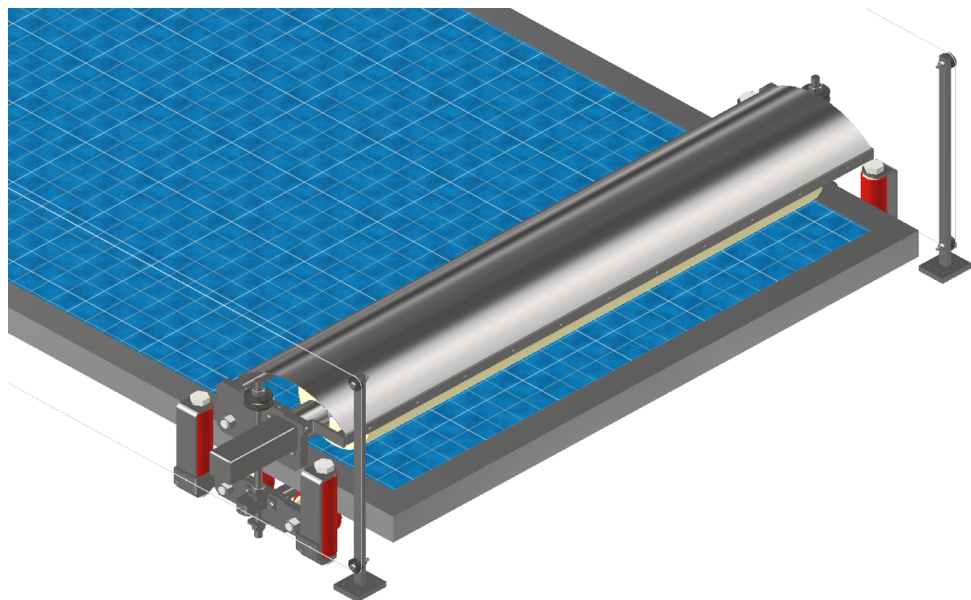


Figure39: Detail of the cleaning system

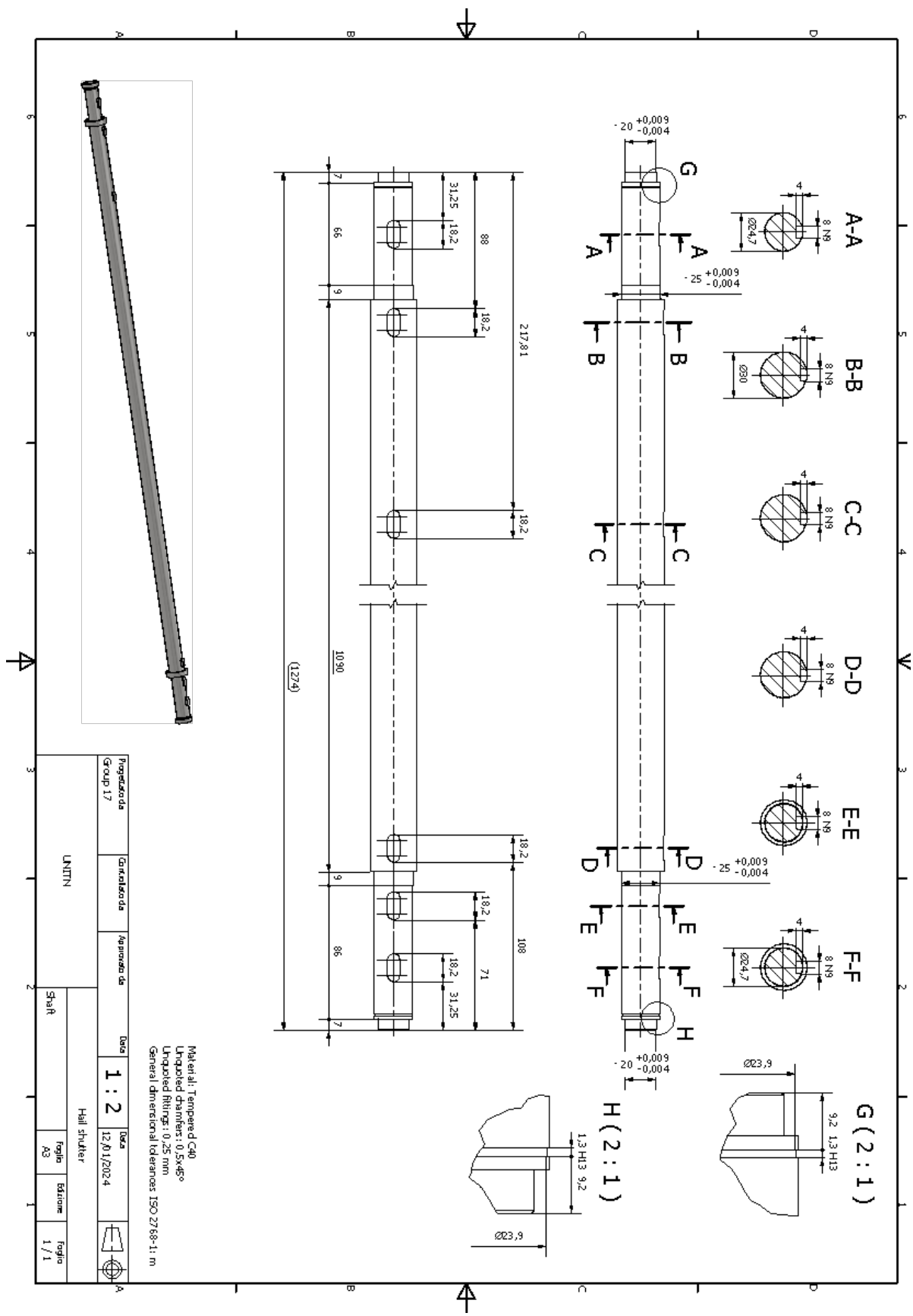


Figure 40: Technical drawing of the shaft

8. REFERENCES AND APPENDICES

- [1] Analysis of dust losses in photovoltaic modules
J. Zorrilla-Casanova^{*1}, M. Piliougue¹, J. Carretero¹, P. Bernaola¹, P. Carpene¹,
L. Mora-López², M. Sidrach-de-Cardona¹
- [2] Rolling bearings, © SKF Group 2018
- [3] Ing. D. Benasciutti, "Richiami di teoria sulle ruote dentate", Corso di Costruzione di Macchine, Dipartimento di Ingegneria Elettrica Gestionale Meccanica (DIEGM), Università degli Studi di Udine
- [4] "General information for use and the maintenance of steel ropes" by Difart srl, Rev. 0 of 05/29/2006
- [5] ref<https://www.jzbrush.com/photovoltaic-dust-removing-roller-brush-for-solar-panel-cleaning-product/>:
- [6] Rauno Holopainen, Eero-Matti Salonen, "Modelling bristle behaviour in rotating brush duct cleaning", Helsinki University of Technology Department of Mechanical Engineering Laboratory of Heating, Ventilating and Air Conditioning, 2003
- [7] L. V. Vanegas-Useche, M. M. Abdel-Wahab, G. A. Parker, "Determination of friction coefficients, brush contact arcs and brush penetrations for gutter brush-road interaction through FEM", Springer-Verlag, 2011
- [8] Ummi Sorfina, Syed Zahurul Islam, Kok Boon Ching, Dur Muhammad Soomro, Jabbar Al-Fatta Yahaya, "Adaptive position control of DC motor for brush-based photovoltaic cleaning system automation", Bulletin of Electrical Engineering and Informatics, Vol. 12, No. 3, June 2023, pp. 1293~1301
- [9] Nasib Khadka, Aayush Bista, Binamra Adhikari, Ashish Shrestha, Diwakar Bista, "Smart solar photovoltaic panel cleaning system", International Conference on Sustainable Energy and Green Technology, 2019
- [10] Micro motors s.r.l
- [11] Misumi Group <https://uk.misumi-ec.com/vona2/detail/221006230444/?HissuCode=ASJ26-10-10>
- [12] BIL Group
- [13] Sodemann molle industriali <https://www.molle-industriali.it/c09751051500s>
- [14] Windowo <https://www.windowo.co.uk/long-nylon-guide-rollers>
- [15] EKD Energy chains